Progress towards an improved Precambrian seawater $^{87}Sr/^{86}Sr$ curve

Xi Chen [a*], Ying Zhou [a], Graham A. Shields [a]

[a] Department of Earth Sciences, University College London, Gower Street, London, WC1E 6BT, UK

* Corresponding Author at: Department of Earth Sciences, University College London, Gower Street, London, WC1E 6BT, UK.

Email Addresses: helen.xi.chen.19@ucl.ac.uk (Xi Chen), y-zhou@ucl.ac.uk (Ying Zhou), g.shields@ucl.ac.uk (Graham A. Shields).

Abstract

The secular trend of seawater strontium isotope ratio ($^{87}Sr/^{86}Sr$) reflects changes in the relative contributions of continental versus mantle reservoirs to ocean composition, and informs global tectonic events, weathering rates and biogeochemical cycling through Earth history. However, the Precambrian seawater $^{87}Sr/^{86}Sr$ curve is known in far less detail than its Phanerozoic counterpart. For this study, we compiled 2249 strontium isotope ratios of Precambrian marine sedimentary rocks published since 2002, alongside previously compiled older data. Here we evaluate the uncertainty of all published data for constraining coeval seawater $^{87}Sr/^{86}Sr$ using four criteria (depositional environment, diagenetic alteration, age constraint and dissolution method). The resultant seawater $^{87}Sr/^{86}Sr$ curve uses mainly 'high certainty' data and shows an overall increasing trend from ~0.7005 at c. 3.5 Ga to ≥0.7089 towards the end of the Ediacaran Period. The improved curve shows an earlier deviation of seawater $^{87}Sr/^{86}Sr$ from the contemporaneous mantle by c. 3.5 Ga, which might reflect the first significant emergence of evolved continental crust related to nascent tectonics. Additionally, the updated curve records two major rises at 2.5-2.2 Ga and 1.9-1.7 Ga in addition to a well-established event at 0.8-0.5 Ga. Despite

the relative scarcity of high-certainty data, these two increases are consistent with enhanced continental weathering following the onset of oxidative weathering and assembly of the supercontinent Nuna, respectively. Although confirmation of these two events awaits more high-certainty data, Precambrian seawater $^{87}Sr/^{86}Sr$ experienced stronger oscillations and better correspondence with supercontinent cycles than previously shown.

Key words

Strontium isotopes; Precambrian; Carbonates; Diagenesis; Dissolution methods; Weathering; Supercontinent cycles

1. Introduction

Strontium isotopes are believed to be homogeneously distributed in seawater on a global scale because the residence time of Sr in the modern ocean (c.10^6 yr) is more than 1000 times longer than the ocean circulation time (Broecker and Peng, 1983; Elderfield, 1986; Hodell et al., 1990). In early studies (Brass, 1976; Faure et al., 1965; Veizer and Compston, 1974), variations in seawater $^{87}Sr/^{86}Sr$ were tied to the weathering of different lithologies. However, since the discovery of hydrothermal exchange as a source of Sr to the ocean (Corliss et al., 1979; Spooner, 1976), the Sr isotope budget of seawater has been interpreted as a balance between more radiogenic riverine input from continental weathering and less radiogenic mantle input from mid-ocean ridges (e.g., Albarède et al., 1981; Corliss et al., 1979; Goldstein and Jacobsen, 1987; Spooner, 1976; Veizer, 1989). The strontium isotope composition of riverine input is complicated by the differential weathering of various lithologies (for example, less radiogenic, more easily weathered basalts versus highly radiogenic, less easily weathered felsic rock) and buffering by the weathering of carbonate rocks with an isotope composition close to seawater (Allègre et al., 2010; Brass, 1976; Galy and France-Lanord, 1999; Veizer and Compston, 1974). Strontium from different sources is homogenized in the ocean and incorporated into authigenic minerals, especially carbonate rocks, via substitution for calcium (McArthur, 1994). A conceptual model of the seawater Sr flux cycle is shown in **Fig.1**.

Strontium isotope stratigraphy (SIS) has come to be widely used in geological studies as a chemostratigraphic tool (Burke et al., 1982; Elderfield, 1986; McArthur, 1994; Veizer et al., 1999), and relies on the observation that the $^{87}Sr/^{86}Sr$ ratio in the world's oceans has varied over time (McArthur et al., 2012). The primary uses of SIS can be summarized as follows: 1) the numerical age of a sample with a known

$^{87}Sr/^{86}Sr$ ratio can be determined by comparison with the global seawater $^{87}Sr/^{86}Sr$ curve (McArthur, 1994; McArthur et al., 2012; 2020); 2) for a sample with known age, its $^{87}Sr/^{86}Sr$ ratio can be used to distinguish pristine from diagenetically altered samples and marine from non-marine settings (e.g., Kuznetsov et al., 2010; Stüeken et al., 2017); and 3) variations in seawater $^{87}Sr/^{86}Sr$ likely reflect long term paleo-weathering conditions and so can be used to test hypotheses of tectonic, biological, and climatic changes through Earth history (e.g., Bartley, 2001; Cawood et al., 2018; Halverson et al., 2007; Hawkesworth et al., 2016; Shields, 2007).

One of the main aims of this review is to explore the relationship between secular changes in seawater Sr isotope composition and Earth system dynamics, including weathering conditions, tectonic events and potentially also oxygenation events. It was initially believed that the seawater $^{87}Sr/^{86}Sr$ curve evolved linearly during geologic history (Wickman, 1948). This assumption was subsequently overturned when researchers realized that the strontium isotope curve oscillated with time (e.g., Burke et al., 1982; Gast, 1955; Veizer and Compston, 1976). While the Phanerozoic curve has been updated repeatedly over the years (e.g., McArthur and Howarth, 2005; McArthur et al., 2012; McArthur et al., 2020) with the abundance of datasets permitting quantification of uncertainties using LOWESS (e.g., McArthur et al., 2012, 2001), further study of the Precambrian curve, defined by only sparse datasets, has lagged behind. Shields and Veizer (2002) published a carbonate geochemistry compilation covering Precambrian time and thereby constructed a seawater strontium isotope curve using in most cases the lowest values of carbonate samples as it was suggested that diagenetic exchange would generally increase measured Sr isotope values. Although that curve is still widely used for reconstructing tectonic cyclicity over time (e.g., Cawood et al., 2018; Hawkesworth et al., 2016), many new data have

been published in the intervening two decades and it has an inadequate temporal resolution. The strontium isotope curve of seawater needs therefore to be periodically updated to keep up with new data and increasingly precise age constraints, which necessitate an updated compilation with more stringent screening.

Reconstructing the Precambrian seawater strontium isotope curve faces a number of critical difficulties such as the high potential for diagenetic alteration, greater age uncertainty, predominance of dolomite in the Precambrian, especially prior to the Neoproterozoic, etc. Moreover, different issues arise in different localities. For instance, continental margin settings, although more likely to be open marine, have generally been affected by tectonic convergence events and ocean closures, resulting in higher metamorphic grade, whereas cratonic interiors, although potentially better preserved, have less precise age constraints, and are more likely to be affected by restricted environments and alteration by meteoric fluids. SIS studies must rely on diagenetically well-preserved chemical precipitates in that post-depositional alteration could alter both chemical and isotopic compositions (Shields and Veizer, 2002). However, well-preserved materials (low-Mg calcitic fossils; such as conodonts and articulate brachiopods) that are widely available in Phanerozoic rocks are absent in Precambrian rocks (Brand and Brenckle, 2001; Kah et al., 2001). Fine-grained bulk carbonate rocks (e.g., micrite) are often used for strontium isotope studies of Precambrian seawater, but their study requires well-honed dissolution methods and screening to obtain the least-altered values (Bailey et al., 2000; Li et al., 2011). Additionally, other problems such as a limited amount of suitable carbonate rocks, ambiguous paleoenvironmental settings (Prokoph et al., 2008; Shields and Veizer, 200; Kuznetsov et al., 2010) also hinder Precambrian SIS studies to some degree. Nevertheless, a growing number of carefully executed studies have shown that

resolution approaching Phanerozoic levels can be achieved under ideal circumstances (e.g., Zhou et al., 2020).

The main aims of this review are:

1) To summarize the different dissolution and diagenetic screening methods used in isotopic studies of Precambrian carbonate rocks in order to demonstrate their advantages and shortcomings.
2) To update an existing Precambrian seawater strontium isotope compilation (Shields and Veizer, 2002), using publications between 2002 and 2020, and apply four criteria (depositional environment, diagenetic alteration, age constraint and dissolution method) to assign both newly and previously compiled data to one of three groups: high-certainty data; medium-certainty data; and low-certainty data. We use the most recent international geologic time scale (Strachan et al., 2020) to assign data to formal time subdivisions.
3) To discuss possible explanations for the temporal trend of the updated curve by reviewing recognizable events (supercontinent cycles, glaciations, large igneous provinces, etc.) and incorporating complementary data sets (Nd, Hf, O isotopes); to provide tests for some highly controversial topics (e.g., the onset of plate tectonics) using the improved Sr isotope curve.

2. Analytical methods

2.1 Sample types for Precambrian SIS

Low-Mg calcitic fossils, such as foraminifera, brachiopods and belemnites, and apatitic fossils, such as conodonts, are abundant in Phanerozoic marine strata. When well preserved, they tend to retain a near original seawater signal, particularly when deposited in carbonate-dominated sediment, and so are ideal materials to reconstruct the Phanerozoic seawater strontium isotope curve (e.g., McArthur et al., 2020; Veizer

et al., 1999). Because no such skeletal material is available for Precambrian SIS, bulk carbonate (e.g., Cox et al., 2016; Halverson et al., 2007) or micro-drilled primary carbonate components, such as calcite cement or homogeneous micrite (e.g., Kaufman et al., 1993; Zhou et al., 2020), are commonly used.

Recrystallization in carbonates generally leads to an increase in grain size, and so the most finely crystalline material, generally micrite, is considered to have escaped substantial diagenetic recrystallization (Kah, 2000a; Kah et al., 1999). Consequently, fine-grained carbonate components, extracted by petrographically guided micro-drilling, are generally recommended for SIS (e.g., Li et al., 2011). Early diagenetic calcite microspar cement or CMC (Zhou et al. 2020, also referred to as "Molar-tooth structure"; e.g., Fairchild et al., 1997; James et al., 1998; Shields, 2002) may also be suitable for SIS where available. CMC is characterized by uniform, equant, polygonal and tightly packed calcite crystals (Furniss et al., 1998; James et al., 1998; Pollock et al., 2006) that filled voids and cracks before deposition of much overlying sediment and before total lithification of surrounding matrix (Fairchild et al., 1997; Smith, 1968). Non-carbonate rocks such as barite (e.g., McCulloch, 1994; Satkoski et al., 2016), gypsum or anhydrite (e.g., Kah et al., 2001) and francolite (Li et al., 2011) have also been used for strontium isotope studies. For instance, in some Archean sedimentary sequences where carbonate is scarce, barite can still be a reliable monitor for seawater Sr isotope composition as it generally has high Sr contents and resists recrystallization (Paytan et al., 1993) as long as its origin can be determined (Griffith and Paytan, 2012). In the following discussion, we mainly focus on carbonate rocks as they are the most commonly used materials for Precambrian SIS.

2.2 Carbonate sample preparation

Significant artefacts in strontium isotope stratigraphy (SIS) studies might result from

159 improper sample preparation that dissolves recrystallised derivates or contaminant
160 components, requiring a suitable dissolution method to minimise the Sr contamination
161 from untargeted phases (McArthur, 1994). We divided dissolution methods of
162 carbonate rocks into three main types: single-step bulk leaching method, two-step
163 sequential leaching method, and multiple-step sequential leaching method. We further
164 subdivided the three main types according to the acid type and reagents used for pre-
165 leaching (ammonium acetate or acetic acid). Details and related references are provided
166 in **Table 1**.

167 Single-step bulk leaching used to be the most common method for carbonate
168 extraction, which is conducted by adding an acid to rock powder to dissolve carbonate
169 minerals, while leaving insoluble detrital phases behind (e.g., Brand et al., 2012; Hall
170 and Veizer, 1996; Kaufman and Knoll, 1995; Kupecz and Land, 1991; Miller et al.,
171 2008). In some cases, carbonate samples are dissolved in a weak acid, such as acetic
172 acid, which is considered to be less aggressive than a dilute strong acid, to avoid
173 dissolution of matrix incorporated impurities (e.g., Kaufman and Knoll, 1995; Miller
174 et al., 2008; Yoshioka et al., 2003), but in other cases, sample powders are dissolved
175 in strong acids such as HCL and HNO_3 (e.g., Brand et al., 2012; Satkoski et al., 2017).
176 The latter method should be avoided, especially for impure samples, because
177 aggressive acid leaching attacks clay minerals in the rock matrix that likely contain
178 Rb and therefore radiogenic Sr from Rb decay, leading to higher measured strontium
179 isotope values (e.g., Bailey et al., 2000).

180 Pre-leaching has been emphasized as it enhances the reliability of obtained values
181 by removing exchangeable Rb and Sr, and strips potentially-contaminating Sr from
182 non-carbonate phases (e.g., Bailey et al., 2000). Pre-leaching has been shown to
183 remove contaminant Sr, even from pure samples. In the experiment of Bailey et al.,

(2000), carbonate samples from Trunch and Lagerdorf were very pure (96% and 98% carbonate, respectively), but only pre-leached samples exhibited near expected seawater values. Such sequential leaching methods started already in the early 90's and are very widely used in strontium isotope studies (Bailey et al., 2000; Bellefroid et al., 2018b; Gorokhov et al., 1995; Kupecz and Land, 1991; Liu et al., 2013; Li et al., 2011).

Based on the ten step leaching experiment of Bailey et al., (2000), later confirmed by Li et al., (2011), the commonly used two-step sequential leaching method suggests using the first leach (pre-leach process, c. 30%-40% dissolved) to remove most contaminant Sr and Rb, followed by a weak acid leach (another c. 30% dissolved) for Sr isotope analysis. This second leach has been shown to provide near primary calcite ratios, importantly leaving the sample incompletely dissolved and the solution at a neutral *p*H to avoid further contamination from other phases. As for the reagents used in pre-leaching, although ammonium acetate is widely used, it might be unnecessary as dilute acetic acid may remove contaminant Sr at least as effectively (e.g., Bailey et al., 2000; Li et al., 2011).

In addition to single-step bulk leaching and two-step leaching, a multiple-step leaching procedure, using acetic acid of intermediate strength, has also been tested. Although relatively complicated, this approach can improve the fidelity of measured $^{87}Sr/^{86}Sr$ values, especially for samples with complex and heterogeneous mineralogy (Bailey et al., 2000; Bellefroid et al., 2018b; Liu et al., 2014, 2013). By measuring elemental concentrations and $^{87}Sr/^{86}Sr$ values for all individual leaching steps, the least-contaminated fraction of each sample can be identified (Bailey et al., 2000; Bellefroid et al., 2018b).

Diverse dissolution methods utilised in the SIS studies (mainly from our new

compilation) have been summarized in **Table 1.**

Type	Pre-leach	Dissolution Method	References	Comments
1. Single-bulk leaching in weak acid without pre-leaching	No pre-leaching	Aliquots of drilled powders are dissolved in weak acid (acetic acid) to avoid dissolution of clastic phases, then centrifuged to separate soluble and insoluble fractions.	Alvarenga et al., 2019, 2014; Bartley et al., 2001; Bekker et al., 2006, 2003b; Galindo et al., 2004; Kaufman and Knoll, 1995; Miller et al., 2008; Sawaki et al., 2010b, 2010a; Yoshioka et al., 2003; Zhang et al., 2020	Preferred for large datasets but lack of pre-leach increases the risk of contamination from ion exchangeable sites and secondary carbonate phases.
2. Single-bulk leaching in strong acid without pre-leaching	No pre-leaching	Powdered carbonate samples are dissolved in strong acid such as HCL and HNO_3	Azmy et al., 2006; Brand et al., 2012; Frauenstein et al., 2009; Nogueira et al., 2007; Satkoski et al., 2017	Dissolving samples in a strong acid might lead to higher $^{87}Sr/^{86}Sr$ by attacking more radiogenic clastic phases.
3. Two-step sequential leaching with pre-leach in ammonium acetate	Pre-leached in aqueous ammonium acetate (NH_4OAc)	Aliquots of powdered carbonate are pre-leached in volumes of ammonium acetate to remove loosely bound Rb and Sr cations, then insoluble residues were leached in acetic acid and the subsequent insoluble residue removed by centrifugation.	Bartley et al., 2007; Bekker et al., 2003a; Bold et al., 2016; Cox et al., 2016; Cui et al., 2015; Gibson et al., 2019; Gorokhov et al., 1995; Halverson et al., 2007; Kochnev et al., 2018; Kuznetsov et al., 2010, 2008, 2005, 2012; Melezhik et al., 2009, 2005; Rooney et al., 2014; Semikhatov, 2002; Semikhatov et al., 2004; Thomas et al., 2004; Valladares et al., 2006	Effectively removes Sr contamination via pre-leach. However, same volume of acid for all samples within a given batch might lead to an acid excess for impure carbonates (Bellefroid et al., 2018b).

4.	Two-step sequential leaching with pre-leach in acetic acid	Pre-leached in dilute acetic acid	After pre-leaching, samples are dissolved partially using acetic acid.	George et al., 2019; Li et al., 2011, 2020; Ray et al., 2003; Zhou et al., 2020	Acetic acid pre-leach might remove contaminant Sr more effectively compared with ammonium acetate (Bailey et al., 2000; Li et al., 2011).
5.	Multiple-step sequential leaching	Pre-leached in volumes of ammonium acetate (NH_4OAc)	Aliquots of powdered carbonate are pre-leached in volumes of ammonium acetate, then the insoluble residues are sequentially leached in acetic acid to identify the most pristine value.	Bailey et al., 2000; Bellefroid et al., 2018b; Fairchild et al., 2018; Li et al., 2020; Liu et al., 2014, 2013	This method is more complicated, but it is more likely to obtain an improved $^{87}Sr/^{86}Sr$, especially for samples with complex mineralogy and heterogeneities (ammonium acetate could be unnecessary if followed by dilute acetic acid)

Table 1. Summary of different dissolution methods of bulk carbonate rocks for strontium isotope analysis. References include the method papers and the newly compiled papers in this study.

3. Diagenetic analysis

3.1. Carbonate diagenesis

Precambrian strontium isotope stratigraphy (SIS) relies on the analysis of well-preserved marine carbonate rocks because post-depositional alteration can alter the chemical and isotope composition of carbonate rocks. Carbonate diagenesis can include dissolution and reprecipitation that affects both the mineralogy and crystal size of the original carbonate precipitate and can occur in different types of fluids such as meteoric or marine fluids (Higgins et al., 2018; Melim et al., 2004; Swart, 2015). The degree of geochemical alteration by diagenesis depends on factors such as the openness and the water-rock ratio of the diagenetic system and the stability of mineralogy (Marshall, 1992; Banner and Hanson, 1990). Open-system and high water-rock ratios generally lead to a greater loss of primary environmental signals (Marshall, 1992). When dissolution takes place in a large volume of pore water, the composition of pore fluids is little influenced by the input of dissolving materials. Thus the composition of replacement phases would be similar to pore fluids that reflect equilibrium with the diagenetic environment (Marshall, 1992; Veizer, 1983). High-magnesium calcite and aragonite are metastable, whereas low-magnesium calcite is relatively insoluble and inherently has less potential for diagenetic exchange (Marshall, 1992; Morse and Mackenzie, 1990; Swart, 2015).

Using static limits of trace elements such as Mn or Sr to select least-altered data has been proposed (e.g., Bates and Brand, 1991; Denison et al., 1994; Montañez et al., 1996). However, it has also been argued that the static threshold inadequately parameterizes the range of diagenetic effects experienced by carbonate components (Brand, 2004; Brand et al., 2012, 2010). It is unlikely that there are any unique criteria for the robust screening of altered samples because the post-depositional history

varies from basin to basin and even from sample to sample within a basin, so using static limits ignores spatial and temporal variations in local conditions (Bartley et al., 2001; Melizhik et al., 2001; Halverson et al., 2007). Therefore, a dynamic approach defined as utilising various screening methods to examine coeval materials from individual horizons is recommended **(Fig. 2),** which generally includes field and petrological examinations, geochemical screening (major and trace elements, stable isotopes, and strontium isotopes) and coeval sample comparisons (e.g., Banner, 2004; Bartley et al., 2001; Brand et al., 2012; Zhou et al., 2020)

3.2. Screening methods

3.2.1. Petrographic screening

Petrographic screening investigates textural or mineralogical changes in rocks using scanning electron microscopy, X-ray diffraction, thin section examination, and cathodoluminescence techniques (McArthur, 1994 and references therein) to distinguish primary from secondary sedimentary components. Primary components such as stromatolitic laminae, micrites, syndepositional marine cement and oolitic grains are most likely to retain original isotopic signals; while secondary components such as cross-cutting veins, late-stage void filling spar and dissolution features should be avoided during sampling (e.g., Kah et al., 2012, 1999; Kaufman and Knoll, 1995). Additionally, siliciclastic material might flag diagenetic alteration because it is normally associated with increased permeability to diagenetic fluids (Kah et al., 1999).

Diagenetic recrystallization processes commonly result in coarsening of grain size or complete obliteration of primary fabrics, if diagenesis took place in the presence of a fluid phase (e.g., meteoric or deep burial fluid) very distinct in composition from seawater. By contrast, fine-grained, primary components that preserve original

textures (e.g., ooids, small-scale sedimentary structure) indicate that recrystallization might have occurred in the presence of fluids similar to the composition of seawater, which means recrystallization/diagenesis occurred synsedimentarily or during shallow burial (Gilleaudeau et al., 2018).

Cathodoluminescence study of polished thick sections provides a qualitative way of estimating alteration (Bartley et al., 2007; Frank et al., 2003; Kah et al., 1999; Kaufman and Knoll, 1995). Luminescence in carbonates is commonly activated by Mn^{2+} and quenched by Fe^{2+} (Hemming et al., 1989). Mn and Fe are commonly rich in meteoric and burial fluids. Thus, this technique can be used to differentiate between samples that have been altered by meteoric and burial diagenesis and samples that have not (Kaufman and Knoll, 1995). Generally, dull, uniform to patchy luminescence indicates primary components, while brightly luminescent to non-luminescent, distinct zoning indicates secondary components (Kah et al., 2012, 1999).

3.2.2. Geochemical screening

1) Major and trace elements

Trends in the concentration of major and trace element such as Mg, Ca, Sr, Fe, and Mn are commonly used to recognize potential alteration in suites of samples (e.g., Denison et al., 1994; Van Geldern et al., 2006; Veizer et al., 1992a, 1992b). Mn/Sr or Fe/Sr are widely used as indices of alteration, and are generally expected to be higher in diagenetically-altered samples than in coeval seawater (Banner and Hanson, 1990; Brand and Veizer, 1980; Gorokhov et al., 1995; Kaufman and Knoll, 1995). This is because the distribution coefficient of Mn and Fe in stable (hexagonal) carbonate minerals (e.g., dolomite and calcite) is much higher than Sr, so recrystallization leads to an increase in Mn/Sr and Fe/Sr ratios (Rimstidt et al., 1998). However, this general relationship is complicated by variable redox conditions, diagenetic fluids, and

mineralogy. High Mn/Sr or Fe/Sr ratios might indicate carbonate precipitation from anoxic waters instead of diagenetic alteration because both Fe and Mn tend to revert to their more soluble reduced forms under suboxic-anoxic conditions (Bruland et al., 2014; Canfield and Thamdrup, 2009). For instance, in low-oxygen Proterozoic oceans, elevated Mn and Fe concentrations could also reflect primary seawater (Bekker et al., 2003b; Gilleaudeau and Kah, 2013; Kah et al., 2004; Kah and Bartley, 2011). Burial diagenetic phases are commonly enriched in Mn and Fe due to reducing conditions in burial fluids (Veizer, 1983), but meteoric diagenetic phases can be characterized by either enrichment or depletion of Mn and Fe due to variable redox conditions in meteoric fluids (Banner and Hanson, 1990; Brand and Veizer, 1980). Moreover, mineralogies also need to be considered. For instance, dolomite generally has a higher preference for Fe and Mn (Mazzullo, 1992) and a lower preference for Sr compared with calcite (Vahrenkamp and Swart, 1990), while some early diagenetic dolomite can also be enriched in Sr relative to Fe and Mn (Gilleaudeau et al., 2018). It is common to use Mg/Ca to quantify the relative contribution of dolomite of samples (e.g., stoichiometric dolomite is generally considered as Mg/Ca ratios of >0.6). Using Mg/Ca ratio in conjunction with Mn/Sr, Fe/Sr could indicate modification of trace elements during dolomitization.

2) Stable isotope composition

The oxygen isotopic composition ($\delta^{18}O$) of carbonate rocks is sensitive to post-depositional alteration resulting from exchange with pore water oxygen and/or recrystallisation at elevated temperatures. The original oxygen isotope composition might be retained where carbonate minerals were subject to only minor recrystallisation under low water-rock ratio conditions (<10; Banner and Hanson, 1990; Jacobsen and Kaufman, 1999). Recrystallization and neomorphism at higher

312 temperatures are generally expected to lower the $\delta^{18}O$ of samples (Veizer, 1983).
313 However, $\delta^{18}O$ composition of meteoric waters is variable, i.e., it becomes lower with
314 decreasing temperature and increasing latitude (Bowen and Wilkinson, 2002).
315 Therefore, meteoric waters will often be not so different to seawater in tropical marine
316 carbonate platform settings. Additionally, dolomitization tends to increase $\delta^{18}O$. For
317 instance, at 25°C the estimates for $\Delta\delta^{18}O_{dolo\text{-}cal}$ (difference in $\delta^{18}O$ between
318 coprecipitated dolomite and calcite) range from 5‰ to 9‰ (Clayton and Epstein,
319 1958), 4‰ to 7‰ (e.g., Degens and Epstein, 1964; Northrop and Clayton, 1966) or
320 2.6‰ (Vasconcelos et al., 2005). Considering the variability of $\delta^{18}O$ in different
321 situations, it needs be used in conjunction with other parameters such as trace element
322 or strontium isotopes to indicate diagenetic alteration.
323 Compared with oxygen isotopes, carbon isotope values ($\delta^{13}C$) are more resistant to
324 overprinting during diagenetic recrystallisation owing to the higher concentration of
325 carbon in carbonate rocks relative to diagenetic fluids (e.g., Halverson et al., 2005).
326 Given water/rock ratios >1000 (Banner and Hanson, 1990), $\delta^{13}C$ values of carbonates
327 might be altered by re-equilibration during recrystallization, whereby interactions
328 with diagenetic fluids would generally decrease $\delta^{13}C$ values because diagenetic fluids
329 potentially contain isotopically depleted carbon. Cross-plots of $\delta^{13}C$ against $\delta^{18}O$
330 values are commonly applied to identify covariation, which might indicate diagenetic
331 alteration (Banner, 1995; Brand and Veizer, 1981). However, authigenic carbonate
332 precipitated from sediment pore fluids that have a different composition from
333 overlying seawater, can produce higher or lower carbonate isotope values than
334 primary carbonate, which complicates the use of $\delta^{13}C$ in identifying diagenetic
335 processes (e.g., Schrag et al., 2013; Sun and Turchyn, 2014; Torres et al., 2020; Zhao
336 et al., 2016)

Mineralogical changes, e.g. recrystallization of aragonite to calcite and dolomite, affect the geochemical indices to some degree (Brand et al., 2012). For instance, an aragonite precursor may cause $\delta^{13}C$ and $\delta^{18}O$ values to shift by +1.8‰ and +0.8‰, respectively, and these signatures could be retained if recrystallisation happened in a closed system (Rubinson and Clayton, 1969; Saltzman, 2005). Dolomitization would increase $\delta^{18}O$ and decrease Ca and Sr concentrations simultaneously, leading to smaller changes to $\delta^{18}O$ values and Sr/Ca, which might erroneously imply a lesser degree of alteration (Halverson et al., 2007).

3) Strontium isotopes

The Sr isotope composition of carbonate minerals is commonly affected by diagenesis; hence $^{87}Sr/^{86}Sr$ ratios can also be used as indicators of alteration in the case that the original Sr isotope composition is known (Gorokhov et al., 1995; Ovchinnikova et al., 1995). In general, post-depositional processes tend to increase $^{87}Sr/^{86}Sr$ values because evolved K-bearing silicates (rich in ^{87}Rb and thus higher $^{87}Sr/^{86}Sr$) release ^{87}Sr into interstitial fluids from where it can be incorporated into carbonate rocks during diagenetic recrystallization (e.g., Fairchild et al., 2018). Therefore, in general, the current best estimates for seawater $^{87}Sr/^{86}Sr$ are based mainly on the least radiogenic samples within a suite of rocks (e.g., Shields and Veizer, 2002). However, fluids that are less radiogenic than contemporaneous seawater, influenced either by mafic components/juvenile silicate, hydrothermal fluids or pressure solution of older, underlying carbonate rocks, may drive carbonate $^{87}Sr/^{86}Sr$ to lower values (e.g., Brand et al., 2010; Cui et al., 2020; Miller et al., 2008; Satkoski et al., 2017). Alternatively, deviation from seawater values might also reflect a mixture of seawater and influence from river catchments in restricted environments (Miller et al., 2008). Therefore, a combination of multiple screening methods and

appropriate leaching methods, as well as careful sample selection and well-constrained geological context, are needed to get a robust result. Elemental and isotopic thresholds used for diagenetic screening compiled from the literature are shown in **Table 2**.

4. Rubidium contamination

The radioactive isotope of Rb, ^{87}Rb, decays to ^{87}Sr over time with a decay constant (λ) of 1.42 x 10^{-11} yr^{-1} (Steiger and Jäger, 1977); thus, the measured $^{87}Sr/^{86}Sr$ values of carbonate rocks increase with radioactive ^{87}Rb decay. Some rubidium may have been incorporated into the carbonate minerals directly, although its large size and 1^+ charge precludes substantial replacement of Ca^{2+} or Mg^{2+} ions in the mineral lattice. Most Rb in sedimentary rocks is incorporated in the structure of igneous minerals and their weathering products as well as potassium-rich clay minerals, which can constitute a substantial portion of some bulk rock samples (McArthur et al., 2012). Therefore, it is common to carry out a correction for Rb decay to estimate the initial $^{87}Sr/^{86}Sr$ value (e.g., Sawaki et al., 2010a; Zhou et al., 2020). However, errors in Rb correction can be introduced because of uncertainty in the samples' ages, especially for Precambrian samples, and because of incongruent leaching of Rb versus Sr. Well-preserved, pure carbonate components will not contain much Rb. Aragonite with its more open structure could accommodate Rb more easily than calcite, but it still incorporates much more Sr, making the Rb/Sr ratios very low and the Rb correction unnecessary (McArthur, 1994). For bulk rock samples, initial $^{87}Sr/^{86}Sr$ ratios may be overcorrected because clay minerals preferentially lose ^{87}Sr from their lattices during diagenesis or leaching procedures compared with the parent Rb (Shields and Veizer, 2002). A good correlation between Rb concentration and Al concentration could demonstrate that Rb derives from aluminosilicates; hence, sample cleaning and pre-leaching is preferable to automatic

387 Rb-decay correction (Gorokhov et al., 1995; Hall and Veizer, 1996; Wierzbowski et al.,
388 2012). To avoid error caused by Rb correction in our compilation, in most cases we
389 directly use the measured values, which, where demonstrably well preserved, must
390 therefore represent near primary maximum constraints on contemporaneous seawater.

Sr (ppm)	Mn/Sr	Fe/Sr	Mg/Ca	$\delta^{18}O_{VPDB}$ (‰)	Sample	Era	Reference
	< 5	< 10			L	NP	Kochnev et al., 2018
	< 0.2		< 0.01		L	NP	Galindo et al., 2004
	≤ 4	≤ 10			L	NP	Kuznetsov et al., 2006
	< 0.2	< 5.0			L	NP	Kuznetsov et al., 2005
	< 0.1				L	NP	Melezhik et al., 2009
				-5~-11	L	NP	Miller et al., 2009
	< 0.2			> -8		NP	Yoshioka et al., 2003
> 400	< 1		< 0.1		L	NP	Gibson et al., 2019
> 500	< 0.1		< 0.01		L	NP	Cox et al., 2016
> 500					L	NP	Bold et al., 2016
≥200	≤0.5		< 0.01		L	NP	Zhou et al., 2020
>1000	<0.6				L	NP	Thomas et al., 2004
	<1 (mostly <0.5)		<0.4 (mostly <0.02)	-5~ -11	L/DL	NP	Halverson et al., 2007

	< 10	< 40			D	NP	Kochnev et al., 2018
	≤ 6	≤ 15			D	NP	Kuznetsov et al., 2006
	≤ 1.2	≤ 3.0	≥ 0.608		D	NP	Kuznetsov et al., 2003b
> 400	< 0.45				D	NP	Alvarenga et al., 2014
	<3			>-11	D/L	NP	Kaufman et al., 1993
>50	< 5			> −10	D	NP	Zhang et al., 2020
	< 0.2	< 5.0	< 0.02	> –10	L	MP	Gorokhov et al., 1995; Kuznetsov et al., 1997; 2008, 2006, 2003a, 2003b; Semikhatov, 2002; Semikhatov et al., 2004;
	< 1.5				L	MP	Bartley et al., 2001
				-6~-9		MP	Bartley et al., 2007
	<1				L	MP	Derry et al., 1992; George et al., 2019

< 3.0	> −10	D	MP	Bartley et al., 2001
< 0.2		L	PP	Kuznetsov et al., 2010
< 2.0		D	PP	Kuznetsov et al.,2010
	-6~-12	D	PP	Bekker et al., 2003a, 2001; Veizer et al., 1992a, 1992b
< 6		D	PP	Kaufman and Knoll, 1995

Table 2. Elemental and isotopic thresholds used to identify suitably well preserved carbonate rock samples in the published literature. L: limestone; D: dolostone; DL: dolomitic limestone. NP: Neoproterozoic; MP: Mesoproterozoic; PP: Paleoproterozoic. Although static thresholds are widely applied in chemostratigraphic studies, they cannot be applied across different studies and need to be justified on a case-by-case basis.

5. Age constraints and data evaluation

5.1. Age constraints

Chemostratigraphic correlation (mainly carbon isotopes) is well-established for the Neoproterozoic (especially Ediacaran), in part due to relatively abundant radiometric ages (i.e., U-Pb, Pb-Pb, Re-Os etc.) and high amplitude carbon isotope fluctuations (Halverson et al., 2010; Kaufman and Knoll, 1995; Knoll et al., 1986). A well-constrained chronostratigraphic framework allows us to assign ages of Neoproterozoic samples with a greater degree of precision. We have put almost all Neoproterozoic datasets into chronostratigraphic in order to get the best-estimated ages based on and updated from the latest age models, such as those of Macdonald et al., (2013), Cox et al., (2016), Bold et al., (2016), Fairchild et al., (2018). In these age models, carbon isotope trends were used by authors to calibrate Sr isotope records to get precise relative ages. In each succession, ages were constructed either by basic thermal subsidence modelling (e.g., Halverson et al., 2002) or by linear interpolation between correlated ages by assuming a constant sedimentation rate (Cox et al., 2016; Zhou et al., 2020).

Unfortunately, the global chemostratigraphic record remains limited for earlier Proterozoic and Archean times, and stratigraphic correlation still faces many challenges. Without well-established global chronostratigraphic frameworks and age models, it is generally not possible to assign ages to earlier Proterozoic and Archean samples in the same way as for the Neoproterozoic. Therefore, we mainly use ages provided by authors (e.g., absolute dates, chemostratigraphic correlation etc.), and update them where any newly-published dating/correlation has become available. We follow Shields and Veizer, (2002), defining age uncertainties less than ±50 Ma as well-constrained, and larger than ±50 Ma as poorly constrained.

5.2. Data evaluation

Four criteria (depositional environment, preservation, age constraints and dissolution methods) are used to assign compiled data to one of high, medium and low-certainty groups **(Table 3, Fig. 3).** The updated strontium isotope curve of Precambrian seawater is based mainly on high-certainty data. Medium-certainty data are also included in the reconstruction for completeness but only contribute to the interpretation of the curve where high-certainty data are not available. Low-certainty data are excluded from the curve reconstruction.

Depositional environment and preservation are essential preliminary criteria for data ranking in this compilation. Samples used to reconstruct the seawater strontium isotope curve have to be deposited in an unrestricted marine environment and record the original seawater signal. Any non-marine or/and diagenetically altered samples would be rated as "low-certainty" and excluded from the curve reconstruction, whether they meet other criteria (i.e., age constraints and dissolution methods) or not.

Age constraints and dissolution methods are used to distinguish "high-certainty" from "medium-certainty" data, but not for defining "low-certainty". A well-constrained age (age uncertainty within ±50 Ma) and appropriate dissolution method (i.e., pre-leaching and using a weak acid, see discussion in section 2.2) provide a greater degree of precision. We define samples that satisfy all four criteria (marine, well-preserved, well-constrained age, appropriate leaching method) as "high-certainty". "Medium-certainty" data are those without well-constrained ages or appropriate leaching method, but still likely containing an original marine signal (i.e., marine environment, well-preserved). "Medium-certainty" data are included to fill some "high-certainty" data gaps in the curve construction and assist the curve interpretation.

Marine environment	Good preservation	Well constrained ages (less than ±50 Ma)	Good leaching method	Certainty rating
Yes	Yes	Yes	Yes	High
Yes	Yes	Not necessarily	Not necessarily	Medium
Not necessarily	Not necessarily	-	-	Low

Table 3. Summary of criteria for data certainty ranking

6. Compilation and curve description

6.1 Compilation

Chemostratigraphic data compilations need continual updating in order to take into account new data, improved age constraints and potentially different screening criteria. For this reason we provide all the relevant isotopic data and metadata in the supplementary materials associated with this paper.

For this study, we compiled 2249 Sr isotope ratios from Precambrian to Cambrian rocks (4000 Ma – 500 Ma) published between 2002 and 2021 from 62 published articles and 3 unpublished articles (**Supplementary Material 1, 3 and Table 4**). We assigned certainty criteria to all published data, including those compiled in Shields and Veizer (2002) **(Supplementary Material 1, Fig. 3)** and we presented data used for the curve construction, i.e., high and medium certainty data, in **Supplementary Material 2 (see Table 5 for structure**). All data have been normalized to a value of 0.71025 for the international isotope standard SRM NBS 987 using the reporting laboratories' measured values over the period of analysis. In most cases, Rb-corrected data were not used in this study.

Recently, several studies have suggested updated seawater strontium isotope curves for different parts of the Precambrian (Neoproterozoic: Zhou et al., 2020, Cox et al., 2016; Mesoproterozoic: Kuznetsov et al., 2008, Kuznetsov et al., 2019;

Paleoproterozoic: Kuznetsov et al., 2021, 2010; Archean: Ravindran et al., 2020, Roerdink et al., 2021, Satkoski et al., 2017) and a SIS study from Kuznetsov et al., (2018) proposed an updated curve for the Proterozoic part. These published curves provide valuable and complementary references for the reconstruction of the Precambrian seawater $^{87}Sr/^{86}Sr$ curve.

6.2 Fundamental descriptions of the updated curve

The updated seawater $^{87}Sr/^{86}Sr$ curve demonstrates an overall increasing trend from ~0.7005 at c. 3.5 Ga to ≥0.7089 towards the end of the Ediacaran Period with three peaks at c. 2.2 Ga, c. 1.65 Ga and c. 0.5 Ga, respectively **(Fig.4).**

The Archean seawater $^{87}Sr/^{86}Sr$ ratio appears to have deviated from the contemporaneous mantle value since at least c. 3.5 Ga (~0.7005) (McCulloch, 1994; Roerdink et al., 2021)**,** followed by a gradual increase until the end of the Archean c. 2.5 Ga when the ratio reached ~0.702 (Kamber and Webb, 2001). In the Paleoproterozoic ocean, the $^{87}Sr/^{86}Sr$ ratio experienced strong oscillations that increased significantly from ~0.702 at c. 2.5 Ga (Kamber and Webb, 2001) to ~0.705 at c. 2.2 Ga (Bekker et al., 2006, 2003a), followed by a drop at c. 2.1 Ga (~0.703) (Bekker et al., 2003b; Kuznetsov et al., 2010). Then, there was a rebound to another peak of ~0.7062 (Veizer and Compston, 1976) at c. 1.65 Ga before a fall to ~0.7046 (Ray et al., 2003) around the Paleoproterozoic - Mesoproterozoic boundary. The overall pattern of the Paleoproterozoic curve in this study shows similarity with that of Kuznetsov et al., (2018). However, the 2.5-2.2 Ga and 1.9-1.7 Ga parts of the curve are mainly composed of medium certainty data, so the shape, duration and acme of these rises need further confirmation once more high-certainty data become available. The Mesoproterozoic $^{87}Sr/^{86}Sr$ values of the new compilation exhibit modest fluctuation from ~0.7046 to ~0.7050 during c. 1.6-1.2 Ga (Gorokhov et al., 1995; Hall

and Veizer, 1996; Kuznetsov et al., 2008, 2005; Pokrovskiy and Vinogradov, 1994; Ray et al., 2003), before a modest rise to ~0.7059 (Gibson et al., 2019; Kuznetsov et al., 2019; Shields, 2002), followed by a slight decrease to ~0.7052 (Semikhatov, 2002) around the Mesoproterozoic to Neoproterozoic transition. The seawater $^{87}Sr/^{86}Sr$ curve then begins rising through multiple fluctuations from the beginning of the Neoproterozoic (~0.7052, Kuznetsov et al., 2017) until the end of the Ediacaran (~0.7089, Sawaki et al., 2010b), with several significant declines at approximately 0.92 Ga, 0.83 Ga, 0.72 Ga and 0.59 Ga respectively.

Column name	Content of Column
Sample ID number	Unique sample number taken from original publication
Sample description	Additional relevant information
Formation	Formation name occasionally including groups, members, etc.
Location	Name of section, borehole and/or region
Country	Name of country
Depth, m	Depth in borehole
Height, m	Stratigraphic height in section
Mineral	C, calcite; D, dolomite; A, anhydrite; B, barite; M, magnesite; P, phosphorite; H, halite
Era	A, Archean; PP, Paleoproterozoic; MP, Mesoproterozoic; NP, Neoproterozoic
Interval	Eras subdivision from Eoarchean to Neoproterozoic
Geon	100 Ma intervals or "Geons" from 0 to 37 (Hofmann, 1999)
Age, Ma	Well-constrained ages (less than ±50 Ma)
Age, Ma	Poorly constrained ages (greater than ±50 Ma)
Uncertainty, Ma	Published age constraints
Source: data	Literature reference for isotopic data (see appendix)
Source: age	Literature references for age constraints
Dating technique	Dating technique, e.g., U-Pb single zircon, biostratigraphy, correlations
Fe, ppm	Iron concentration in carbonate phase, ppm
Mg/Ca	Mg/Ca ratio of carbonate phase
Mg, ppm	Magnesium concentration in carbonate phase, ppm
Ca, wt %	Calcium concentration in carbonate phase, weight%
Mn, ppm	Manganese concentration in carbonate phase, ppm
Sr, ppm	Strontium concentration in carbonate phase, ppm
$\delta^{13}C_{calcite}$ PDB	Carbon isotope composition of calcite, ‰ $_{PDB}$
$\delta^{13}C_{dolomite}$ PDB	Carbon isotope composition of dolomite, ‰ $_{PDB}$
$\delta^{13}C_{others}$ PDB	Carbon isotope composition of other carbonate minerals, ‰ $_{PDB}$

$\delta^{18}O_{calcite}$ PDB	Oxygen isotope composition of calcite, ‰ $_{PDB}$
$\delta^{18}O_{dolomite}$ PDB	Oxygen isotope composition of dolomite, ‰ $_{PDB}$
$\delta^{18}O_{others}$ PDB	Oxygen isotope composition of other carbonate minerals, ‰ $_{PDB}$
$^{87}Sr/^{86}Sr_{measured}$	Reported strontium isotope composition of carbonate phase
$^{87}Sr/^{86}Sr_{initial}$	Strontium isotope composition of carbonate phase after Rb correction
$^{87}Sr/^{86}Sr_{norm.}$	$^{87}Sr/^{86}Sr$ normalised to SRM NBS 987 = 0.71025
Rb, ppm	Rubidium concentration in carbonate phase, ppm
Comments	Comments on data in four aspects (depositional environment, diagenetic alteration, age constraints and leaching approach)
Rating (high-certainty)	Marine environment, least altered, well age constraints, appropriate leaching method (pre-leached, weak acids)
Rating (medium-certainty)	Marine environment, least altered, poor age constraints or/and inappropriate leaching method (no-preleaching, using strong acids)
Rating (low-certainty)	Non-marine or/and diagenetic altered

Table 4. Structure of Precambrian strontium isotope database version 2021 (a). This version includes 2249 newly-compiled data of this study and previous compilation of Shields and Veizer, (2002), whereby the structure is inherited from the PMCID (Precambrian marine carbonate isotope database) version 1.1 (a) of Shields and Veizer, (2002), but adding detailed comments and certainty rating.

Column name	Content of Column
Sample ID number	Unique sample number taken from original publication
Formation	Formation name occasionally including groups, members, etc.
Country	Name of country
Era	A, Archean; PP, Paleoproterzoic; MP, Mesoproterozoic; NP, Neoproterozoic
Interval	Eras subdivision from Eoarchean to Neoproterozoic
Age, Ma	Ages of samples, all samples ages are up to data
Source: data	Literature reference for isotopic data (see supplementary material 3)
$^{87}Sr/^{86}Sr_{norm.}$	$^{87}Sr/^{86}Sr$ normalised to SRM NBS 987 = 0.71025
Rating (high-certainty)	Marine environment, least altered, well age constraints, appropriate leaching method (pre-leached, weak acids)
Rating (medium-certainty)	Marine environment, least altered, poor age constraints or/and inappropriate leaching method (no-preleaching, using strong acids)
New data	High and medium certainty data from this study
Old data	High and medium certainty data from PMCID of Shields and Veizer (2002)

Table 5. Structure of Precambrian strontium isotope database version 2021 (b).This version shows data used for reconstruction of Precambrian seawater $^{87}Sr/^{86}Sr$ curve, which includes high and medium certainty data from both this study and Shields and Veizer (2002).

7. Discussion on the updated $^{87}Sr/^{86}Sr$ curve of Precambrian seawater

Continental chemical weathering exports cations to the ocean and so is one of the key processes influencing not only the evolution of seawater $^{87}Sr/^{86}Sr$ but also the long-term carbon cycle and climate through the consumption of atmospheric CO_2 (Berner, 2003; Berner et al., 1983; Walker et al., 1981). Rb preferentially accumulates in granitic melts due to the relative incompatibility of Rb compared with Sr, resulting in Rb enrichment (high Rb/Sr ratios, thus high ^{87}Sr) in the continental crust and Rb depletion (low Rb/Sr ratios, thus low ^{87}Sr) in the residual mantle and oceanic crust. Secular changes of $^{87}Sr/^{86}Sr$ in the ocean record the relative importance of radiogenic strontium derived from continental crust versus unradiogenic strontium derived from hydrothermal alteration of oceanic crust and so could track the long-term changes in Earth's subaerial weathering. Sr isotope ratios in seawater are affected not only by changes in the rates of continental weathering versus sea-floor spreading (normally associated with supercontinent cycles) but also by changes in the $^{87}Sr/^{86}Sr$ composition of rocks undergoing weathering (generally associated with emplacement of large igneous provinces, crust reworking etc.), which has an intimate association with Earth system dynamics.

Here we show our updated Sr isotope curve against the background of zircon abundance and the supercontinent cycle **(Fig. 5A),** incorporating also Nd, Hf and O isotopes **(Fig. 5B)** and a compilation of collective sizes of large igneous provinces (LIPs; **Fig. 5C**). Peaks in U-Pb zircon crystallisation ages are linked to the amalgamation stages of the supercontinent cycle (Bradley, 2011; Condie, 2004; Condie et al., 2011; Rino et al., 2004). These peaks have been suggested also to have been a consequence of a preservation bias inherent in the supercontinent cycle, whereby high volumes of magma are generated along subduction zones, but the

528 preservation potential of crust generated in collisional orogens is greater (Cawood et
529 al., 2013; Condie et al., 2011; Hawkesworth et al., 2009). The zircon / supercontinent
530 record provides important clues to interpreting secular Sr isotope changes.
531 Supercontinent assembly is thought to be associated with tectonic collision and uplift,
532 resulting in higher erosion rates and therefore an increase in seawater $^{87}Sr/^{86}Sr$.
533 Conversely, rifting and opening of new basins during supercontinent fragmentation
534 might increase input of less radiogenic hydrothermal fluxes into the ocean, driving
535 down seawater $^{87}Sr/^{86}Sr$ (Asmerom et al., 1991; Kaufman et al., 1993; Raymo et al.,
536 1988). However, input fluxes are not always primary controls for marine Sr isotope
537 records, sources of Sr (older and radiogenic crust versus juvenile crust) undergoing
538 continental weathering could also be controlling factors (Bartley et al., 2001; Bataille
539 et al., 2017; Halverson et al., 2007).
540 Isotopic proxies such as εHf and $\delta^{18}O$ in zircons and εNd in whole-rock sediments
541 and granitoids, and the emplacement of large igneous provinces could reflect types of
542 rocks (lithologies) undergoing weathering. εHf and εNd values express the relative
543 deviation of $^{176}Hf/^{177}Hf$ and $^{143}Nd/^{144}Nd$ ratios of a sample from the contemporaneous
544 chondritic uniform reservoir (CHUR) respectively (White, 2015). εHf values in
545 zircons and εNd in whole-rock sediments and granitoids record the degree to which
546 the magma contains the juvenile mantle (high values) versus the reworked crust (low
547 values) (Condie and Aster, 2013). Mantle-derived magmas have relatively low $\delta^{18}O$
548 (5.3±0.3‰; Valley, 2003), whereas magmas that include a contribution from
549 sedimentary rocks have elevated $\delta^{18}O$ because rocks that have experienced a
550 sedimentary cycle or low-grade hydrothermal alteration will have experienced
551 isotopic exchange with water at low temperatures (c. 7–25‰; Eiler, 2001). Thus,
552 elevated $\delta^{18}O$ values in zircon are proposed as a ‘fingerprint’ for the generation of

553 felsic igneous rocks (Hawkesworth et al., 2010). Increasing εHf and εNd values, and
554 decreasing $\delta^{18}O$ values with time reflect more significant input of juvenile crust with
555 unradiogenic Sr isotope ratios; conversely, decreasing εHf and εNd values, and high
556 $\delta^{18}O$ values reflect reworking of older crust with high Sr isotope ratios (Belousova et
557 al., 2010; Collins et al., 2011; Condie and Aster, 2013).

558 Large igneous provinces represent large volumes (>0.1Mkm^3; frequently
559 above>1Mkm^3) of mafic lavas, typically in less than a few million years (Bryan and
560 Ernst, 2008; Coffin and Eldholm, 1994; Ernst and Ernst, 2014). LIP (or continental
561 flood basalt) weathering plays an important role in regulating seawater $^{87}Sr/^{86}Sr$ and
562 global climate due to ~5-10 times greater weatherability of basalts than felsic
563 continental crust (White and Brantley, 1995). Rapid chemical weathering of LIPs
564 delivers unradiogenic Sr into the ocean, leading to a decrease in marine $^{87}Sr/^{86}Sr$ and
565 CO_2 drawdown (Cox et al., 2016; Dessert et al., 2001). The importance of basalt
566 weathering is especially noted for the early-middle Neoproterozoic and Phanerozoic
567 fluctuations in seawater $^{87}Sr/^{86}Sr$ (Bataille et al., 2017; Cox et al., 2016; Gernon et al.,
568 2016; Godderis et al., 2003; Jagoutz et al., 2016; Prokoph et al., 2013). For instance,
569 major strontium isotope falls in the middle Neoproterozoic and middle-late Ordovician
570 were suggested to have been due to enhanced volcanic weathering that potentially
571 triggered the Sturtian and late Ordovician glaciations (Cox et al., 2016; Shields et al.,
572 2003; Young et al., 2009). It is worth noting that evolving palaeogeography is another
573 potential control over seawater $^{87}Sr/^{86}Sr$. Continental lithologies and global climatic
574 zonation vary spatially; thus, ongoing continental drift would lead to changes in the
575 average $^{87}Sr/^{86}Sr$ signature of continental runoff and thus of the ocean (Goddéris et al.,
576 2017).

577 In this section, we will discuss possible explanations for the temporal trend of the

updated seawater Sr isotope curve combining recognizable events and complementary data sets, and will propose plausible hypotheses for some highly controversial topics (e.g., onset of plate tectonics) using this improved curve.

7.1. Archean (4.0-2.5 Ga)

Plate tectonics is a defining characteristic of the modern Earth System that involves a globally linked system of lateral motion of rigid surface plates with lithosphere formed at mid-ocean ridges and consumed in subduction zones. When and whether modern style plate tectonics operated during the Archean remain topics of considerable debate and rigorous research (Brown et al., 2020; Cawood et al., 2018, 2006; Dhuime et al., 2015, 2012; Ernst et al., 2016; Greber et al., 2017; Griffin et al., 2014; Harrison et al., 2008; Hawkesworth et al., 2017, 2010, 2020; Hopkins et al., 2008; Keller and Harrison, 2020; Komiya et al., 1999; Kröner and Layer, 1992; Lipp et al., 2021; Moyen et al., 2006; Nutman et al., 2002; Smithies et al., 2007; Stern, 2018; M. Tang et al., 2016; Taylor and McLennan, 1985; Van Kranendonk, 2010; Van Kranendonk et al., 2007; Windley et al., 2021). Many authors have suggested that plate tectonics commenced during Meso- to Neoarchean times, around 3.2–2.5 Ga (e.g., Brown et al., 2020; Cawood et al., 2018; Dhuime et al., 2015; Hawkesworth et al., 2020, 2017; Tang et al., 2016; Taylor and McLennan, 1985). However, a contrasting view supports an earlier onset of plate tectonic before 3.5 Ga and as early as the Hadean (e.g., Greber et al., 2017; Harrison et al., 2008; Keller and Harrison, 2020; Lipp et al., 2021; Windley et al., 2021). Others argue that modern style plate tectonics began only in the Neoproterozoic Era (Stern, 2018). A detailed discussion on different hypotheses of plate tectonics lies outside the scope of this review, but the updated seawater Sr isotope curve may provide an additional viewpoint from which to appreciate the debate.

The Earth's crust was originally mafic but eventually evolved into two compositionally distinct components: thin, dense, silica-poor oceanic crust and thicker, buoyant, silica-rich continental crust. This dichotomy is generally accepted as maintained by plate tectonics. Thus changes in upper-crust composition (development of felsic crust) are suggested to be a piece of geological evidence for plate tectonic commencement (Greber et al., 2017; Lipp et al., 2021; Tang et al., 2016; Windley et al., 2021). Due to the higher Rb/Sr (higher ^{87}Sr) in silica-rich continental crust than oceanic crust, deviation of seawater Sr isotopes from the contemporaneous mantle has been related to the emergence and weathering of evolved continental crust (Flament et al., 2013). The modelled Sr isotope evolution in the depleted mantle **(Fig. 6)** shows a linear increase to the present-day value of c. 0.7026 with a constant Rb/Sr ratio of ~0.016 (Workman and Hart, 2005). The compilation of Shields and Veizer (2002) indicated that the seawater $^{87}Sr/^{86}Sr$ curve might have deviated from the predicted value for mantle evolution before c. 2.5 Ga and as early as ~2.9 Ga **(Fig. 6).** Our updated compilation, however, shows an earlier deflection before c. 3.5 Ga, after considering data from recent studies such as Roerdink et al., (2021), Ravindran et al., (2020) and Satkoski et al., (2017, 2016). The emerging Sr isotope curve implies that the onset of continental weathering of more evolved crust began before 3.5 Ga and could even have begun as early as 3.7 Ga (Roerdink et al., 2021). The early deviation of the seawater $^{87}Sr/^{86}Sr$ curve might provide support for the earlier crustal differentiation and plate tectonics onset model (before 3.5 Ga). However, it is challenging to discern the role of continental weathering this far back in time, based solely on Sr isotopes, because early continental crust, while differentiated, would have had little time to grow more ^{87}Sr and would remain isotopically very similar to the mantle for over a billion years. Therefore, the leverage of continental weathering to

628 modify seawater composition was much reduced in the Archean such that relatively
629 small changes, once verified, can be considered significant.
630 Titanium (Ti) isotope composition in shale is an alternative way to constrain the
631 chemical composition of the continental crust exposed to weathering. The $^{49}Ti/^{47}Ti$
632 ratio (expressed as $\delta^{49}Ti$; part per mil deviation of the $^{49}Ti/^{47}Ti$ ratio in a sample from
633 that of the Origins Laboratory Ti reference material) is associated with SiO_2
634 concentration because during fractional crystallization, light Ti is preferentially
635 incorporated in Fe-Ti oxides (Millet et al., 2016). For instance, mafic rocks and
636 komatiites have near bulk silicate Earth values [+0.005 ± 0.005 (‰), 95% c.i], while
637 $\delta^{49}Ti$ in evolved rocks has a higher value of +0.6‰ (at SiO_2 concentration of 75%;
638 Greber et al., 2017). Although the Ti concentration of mafic rocks is much higher than
639 that of felsic rocks, Greber et al. (2017) shows that the average $\delta^{49}Ti$ value of shales is
640 almost constant and always higher than that of basalt and komatiites during the past
641 3.5 Ga, indicating that emergent crust was likely dominated by felsic (silica-rich)
642 rocks as far back as 3.5 Ga. The gradual increase of $^{87}Sr/^{86}Sr$ ratios in Paleoarchean
643 seawater also coincides with the widespread occurrence of granitoid-rich crust in the
644 western Dharwar, Kaapvaal and Pilbara cratons and the presence of detrital deposits
645 with felsic sources (Hessler and Lowe, 2006), suggesting that the marine Sr budget
646 started to be dominated by crustal-derived, more radiogenic materials (Ravindran et
647 al., 2020).
648 Plate tectonics would eventually produce supercontinents, thicken the lithosphere
649 and increase crustal reworking (Cawood et al., 2013; Flament et al., 2013;
650 Hawkesworth et al., 2016; Spencer et al., 2014). The subsequent assembly of the first
651 putative supercontinent Kenorland at c. 2.7-2.6 Ga (Williams et al., 1991; Bleeker, 2003)
652 produced collisional orogens that were susceptible to subaerial weathering, potentially

increasing further the flux of radiogenic ^{87}Sr to the ocean during the Neoarchean.

7.2. Proterozoic (2.5-0.54 Ga)

7.2.1. Paleoproterozoic (2.5-1.6 Ga)

The Paleoproterozoic Era is marked by a substantial increase in the oxygen content of the atmosphere at c. 2.4-2.3 Ga (e.g., Bekker et al., 2004; Bekker and Holland, 2012; Canfield et al., 2013; Holland, 2002; Karhu and Holland, 1996; Poulton et al., 2021; Rye and Holland, 1998; Walker et al., 1983); widespread glaciations (e.g., Barley et al., 2005; Kopp et al., 2005; Young, 1991), the Earth's largest positive carbon isotope excursion (Baker and Fallick, 1989; Martin et al., 2013; Melezhik et al., 2005; Schidlowski et al., 1975); the oldest microfossils diagnostic of cyanobacteria and eukaryotes (Hofmann, 1976; Javaux et al., 2013; Javaux and Lepot, 2018; Knoll et al., 2006; Knoll and Golubic, 1992) and sustained plate tectonics (e.g., Cawood et al., 2018; Hawkesworth et al., 2020; Taylor and McLennan, 1985).

The Paleoproterozoic seawater $^{87}Sr/^{86}Sr$ curve appears to have oscillated markedly with two increases at 2.5-2.2 Ga and 1.9-1.7 Ga, respectively. Although the first dramatic increase of $^{87}Sr/^{86}Sr$ from 2.5 Ga to 2.2 Ga is relatively poorly constrained, it coincides with important Earth System events, such as the first accumulation of atmospheric O_2 (the Great Oxidation Episode or GOE; Poulton et al., 2021) and a series of extensive glaciations (c. 2.45-2.22 Ga) . Contributing factors to the rise in seawater $^{87}Sr/^{86}Sr$ include: 1) a decrease in mantle input flux; 2) an increase in the Sr isotopic composition of rocks undergoing weathering; and 3) an increase in continental weathering flux. However, the interval 2.5-2.2 Ga corresponds to a relative low in the zircon age abundance record and sits in a quiet transition before a period of widespread magmatism and rifting, related in part to the breakup of Kenorland at 2.2-2.1 Ga. An increase in the Sr isotope composition of rocks

678 undergoing weathering is plausible, as more felsic crust might have been produced
679 during this period (Dhuime et al., 2015; Lee et al., 2016). However, there is no
680 obvious evidence from Hf, Nd and O isotopes **(Fig. 5B),** so it might not be a primary
681 control for such a dramatic Sr isotope rise**.** We therefore consider a role for an
682 enhanced chemical weathering rate, probably driven by several possible factors, such
683 as increased emergence of continental crust (e.g., Flament et al., 2013), maximised
684 mineral surface area during glaciations (Hallet et al., 1996; Koppes and Montgomery,
685 2009) and oxidative weathering of pyrite (producing sulfuric acid) during the GOE
686 (Bekker and Holland, 2012; Bachan and Kump, 2015; Torres et al., 2014).
687 A thickened lithosphere and largely emergent low-latitude continental crust during
688 the early Proterozoic (c. 2.5 Ga) likely increased the surface area exposed to
689 weathering (Flament et al., 2013; Lee et al., 2016), potentially contributing to the
690 dramatic increase of seawater $^{87}Sr/^{86}Sr$ at ~2.5 Ga. Modelled evolution of P
691 concentrations in Earth's emerged crust through time by Greber et al., (2017) shows a
692 50% increase in the concentration of P (from 0.10 to 0.15 wt% P_2O_5) across the
693 Archean- Proterozoic boundary (2.5 Ga), which could be a result of enhanced
694 continental weathering during this period. As a major limit to biological productivity
695 over geological time scales (Lenton and Watson, 2004; Tyrrell, 1999), an increase in
696 the flux of P from chemical weathering could have led to an expansion of oxygenic
697 photosynthesis and therefore a rise in atmospheric O_2 at c.2.4 Ga **(Fig. 5D).**
698 As for the Sr isotope peak at ~2.3-2.2 Ga, the onset of pyrite weathering
699 (producing sulfuric acid) (Bekker and Holland, 2012; Torres et al., 2017, 2014) may
700 have contributed significantly to the rise to values as high as ~0.705 (Bekker et al.,
701 2006, 2003a). The generation of sulfuric acid (H_2SO_4) from pyrite weathering would
702 have decreased the *p*H of soil and groundwater, inducing the dissolution of rocks and

703 minerals, including apatite, and giving rise to further chemical weathering through net
704 production of CO_2 (Guidry and Mackenzie, 2003; Konhauser et al., 2011; Torres et
705 al., 2017). Additionally, glacial flour could have maximised the surface area exposed
706 to weathering (Anderson, 2007; Hallet et al., 1996; Herman et al., 2013; Koppes and
707 Montgomery, 2009). Therefore, we propose that increased sulfuric acid and largely
708 exposed reactive surface area during glaciation might have resulted in an increased
709 radiogenic Sr flux from the continent.

710 Afterwards, a sharp $^{87}Sr/^{86}Sr$ fall between c. 2.2 Ga to c. 2.1 Ga might be attributed
711 to an increased flux of less radiogenic strontium from mid-ocean ridges and rift
712 volcanism, associated with the final breakup of the Kenorland at 2.2-2.1 Ga (Aspler
713 and Chiarenzelli, 1998; Wanke and Melezhik, 2005), as well as a decreased flux of
714 more radiogenic riverine strontium due to peneplanation of Kenorland. The
715 subsequent second sharp rise of $^{87}Sr/^{86}Sr$ ratios after c. 2.0-1.9 Ga, reaching a peak at
716 c. 1.7 Ga, is concurrent with the amalgamation of the supercontinent Nuna **(Fig. 5A)**
717 and was likely related to global-scale collisional events (Bradley, 2011; Zhao et al.,
718 2004, 2002). It has long been proposed that tectonic-related uplift could facilitate
719 erosion and chemical weathering (e.g., Raymo et al., 1988; Ruddiman and Prell,
720 1997), thus, increasing the continental Sr flux into the ocean. Moreover, the low εHf
721 values of detrital zircons, low Nd isotope ratios in whole-rock sediments and
722 granitoids and zircon $\delta^{18}O$ values during this period imply a contribution from
723 reworked crust with presumably higher $^{87}Sr/^{86}Sr$ ratios (Condie and Aster, 2013;
724 Hawkesworth et al., 2016; Cawood et al., 2018). The following drop of $^{87}Sr/^{86}Sr$ ratios
725 to around 0.7046 at c. 1.6 Ga occurred at the transition from the Paleoproterozoic Era
726 to the Mesoproterozoic Era, implying an increased input of unradiogenic sources,
727 possibly related to the onset of a partial breakup of Nuna (Anderson, 1983; Rogers

728 and Santosh, 2002; Zhao et al., 2004). Simultaneously, εHf and εNd values both show
729 an increasing trend, coupled with decreasing zircon $\delta^{18}O$ values, probably indicating a
730 gradual transition from reworked crust to more juvenile crust during this period (**Fig.**
731 **5B)**.

732 *7.2.2. Mesoproterozoic (1.6 Ga-1.0 Ga)*

733 The middle portion of the Proterozoic Eon (1.8 to 0.85 Ga) is characterised by its
734 relative environmental, evolutionary, and lithospheric stability (e.g., Cawood and
735 Hawkesworth, 2014) with a paucity of passive margins (Bradley, 2008), absence of
736 glaciation (Bradley, 2011) and muted variability in the geochemical record (e.g.,
737 Bartley and Kah, 2004; Brasier and Lindsay, 1998; Buick et al., 1995; Shields, 2007).
738 However, following further detailed studies conducted in recent years, more and more
739 mysteries of this so-called "Boring Billion" have been revealed in terms of eukaryotic
740 evolution (e.g., Adam et al., 2017; Butterfield, 2000; Butterfield et al., 1990; Javaux
741 et al., 2001; Knoll, 2014, 1994; Lamb et al., 2009; Miao et al., 2019; Shi et al., 2017;
742 Tang et al., 2020; Zhang et al., 2018b; Zhu et al., 2016), global tectonic
743 reorganisations (Anderson, 1983; Condie, 2020; Evans and Mitchell, 2011; Huang et
744 al., 2019; Rogers and Santosh, 2002; Zhao et al., 2004), surface O_2 dynamics (e.g.,
745 Diamond et al., 2018; Gilleaudeau and Kah, 2015; Johnston et al., 2005; Kah et al.,
746 2001, 1999; Kah and Bartley, 2011; Liu et al., 2021) and possible carbon isotope
747 excursions (e.g., Bartley et al., 2001; Kah et al., 1999; Knoll et al., 1995; Zhang et al.,
748 2016)

749 The updated strontium isotope curve for Mesoproterozoic seawater shows
750 relatively low values (~0.7045-0.705) with only muted variability between 1.6 Ga-
751 1.2 Ga. The low $^{87}Sr/^{86}Sr$ ratios are concurrent with the fragmentation of the
752 supercontinent Nuna, which began at c. 1.6 Ga with continental rifting and anorogenic

magmatism until its final breakup at about 1.2 Ga with widespread emplacement of mafic dike swarms (Anderson and Arthur, 1983; Rogers and Santosh, 2002; Zhao et al., 2004). The above-zero εHf and εNd curves and low $\delta^{18}O$ **(Fig. 5B),** alongside previous studies, indicate that this period was under the influence of considerable amounts of juvenile mantle-derived rocks and associated hydrothermal systems (Condie and Aster, 2013; Hawkesworth et al., 2016; Semikhatov, 2002). Additionally, 1.6-1.2 Ga also witnessed the emplacement of several large igneous provinces **(Fig. 5C)**, such as the ~1267 Ma Mackenzie LIP, ~1385 Ma Mashak LIP (and other coeval LIPs) and ~1501 Kuonamka LIP etc. (Ernst and Youbi, 2017). The low marine $^{87}Sr/^{86}Sr$ ratios during this period, together with evidence from complementary datasets (εHf, εNd and $\delta^{18}O$, LIPs) suggest that a significant juvenile crust was likely involved in mountain building, and continental weathering was dominated by juvenile less radiogenic crust over ancient, more radiogenic continental crust.

A subsequent increase of $^{87}Sr/^{86}Sr$ since c. 1.2 Ga towards the end of the Mesoproterozoic coincides with amalgamation of the supercontinent Rodinia (Spencer et al., 2013). Weathering conditions during this period were less-constrained previously, but enhanced chemical weathering towards the end of the Mesoproterozoic Era has been proposed recently by Gibson et al., (2019), who related a rise in $^{87}Sr/^{86}Sr$ at ca. 1050 Ma to weathering of Grenville-aged orogens (linked to amalgamation of supercontinent Rodinia). However, in our compilation **(Fig. 5A)**, the incremental rise of $^{87}Sr/^{86}Sr$ during assembly of Rodinia contrasts with the sharp increase during the earlier assembly of Nuna and later assembly of Gondwana, which might indicate that the weathering of materials with relatively low $^{87}Sr/^{86}Sr$ ratios may have predominated even during periods of uplift and erosion. Semikhatov (2002) proposed several possible reasons, such as juvenile magmatism, an extremely arid

778 climate, or the paleogeographic lock-up of continental runoff, whereby collisional
779 orogens at continental margins represented barriers for the terrestrial material
780 transported by rivers. The first reason seems plausible considering the overall high
781 juvenile crust production, which is marked by relatively radiogenic Nd and Hf isotope
782 signatures, and LIPs such as the c. 1005 Ma Sette Daban event (Ernst and Youbi,
783 2017).

784 *7.2.3. Neoproterozoic (1.0 Ga-0.54 Ga)*

785 The Neoproterozoic Era is characterised by climatic vicissitudes, including two
786 prolonged global glaciations during the Cryogenian Period and short-lived, regional
787 ice ages during the Ediacaran Period (e.g., Hoffman et al., 2017; Young et al., 2015
788 and references therein), biological radiations (e.g., Narbonne, 2005; Xiao and
789 Laflamme, 2009), the eruption of large igneous provinces (LIPs) (e.g., Cox et al.,
790 2016; Ernst and Youbi, 2017), oscillations of carbon isotopes (e.g., Halverson et al.,
791 2005; Rothman et al., 2003), ocean oxygenation events (e.g., Shields-Zhou and Och,
792 2011) and tectonic reorganization including fragmentation of the supercontinent
793 Rodinia and subsequent assembly of Gondwana (e.g., Condie and Puetz, 2019;
794 Merdith et al., 2017).

795 A sustained increase in continental weathering rate was believed to be a major
796 contributing factor driving increased $^{87}Sr/^{86}Sr$ ratios in Neoproterozoic seawater
797 (Shields, 2007). However, Halverson et al., (2010) pointed out that some notable
798 trends superimposed on the long term "base-level shift" of marine $^{87}Sr/^{86}Sr$ values,
799 such as the decline prior to Cryogenian glaciation, could tentatively be assigned to the
800 weathering of widespread flood basalts. Coincidently, Bataille et al., (2017) found
801 that $^{87}Sr/^{86}Sr$ changes in igneous rocks were generally well correlated with changes to
802 seawater $^{87}Sr/^{86}Sr$ over the last 1.0 Ga, which indicates that the isotope composition of

weathering input might have played an important role in shaping the seawater $^{87}Sr/^{86}Sr$ curve during this period. Additionally, many researchers have also proposed a critical role for large igneous provinces (LIPs) in determining seawater $^{87}Sr/^{86}Sr$ ratios due to the higher weatherability of basalt (e.g., Cox et al., 2016). Enhanced silicate weathering of unradiogenic, low latitude LIPs likely led to steep dips in the strontium isotope curve. For instance, the falls of $^{87}Sr/^{86}Sr$ ratios at 0.92 Ga, 0.83 Ga, 0.72 Ga could have resulted from the weathering of the Dashigou, Guibei and Franklin LIPs, respectively (Ernst and Youbi, 2017; Zhou et al., 2020). Accelerated uptake of CO_2 via LIP weathering might outweigh the climatic effects of CO_2 degassing, triggering glaciations, such as the Sturtian glaciation (Cox et al., 2016; Ernst and Youbi, 2017; Rooney et al., 2014). Conversely, continental drift (changing palaeogeography) might diminish LIP weathering, allowing seawater $^{87}Sr/^{86}Sr$ to rise again. For instance, numerical models suggest the southward drift of the Franklin LIPs outside the original tropical convergence zone (Li et al., 2013), decreasing its contribution to total Sr flux of continental silicate weathering from 4.5% at 720 Ma to 2.5% at 680 Ma and 635 Ma, which could be a potential reason for the rise of $^{87}Sr/^{86}Sr$ after 635 Ma (Goddéris et al., 2017).

The relatively low values of $^{87}Sr/^{86}Sr$ (c.0.7055-0.7060) during 0.95-0.85 Ga coincided with the tenure of the supercontinent Rodinia (Bradley, 2011). Evidenced by the increasing values of εHf and εNd, the low strontium isotope values during this period might reflect input of less radiogenic strontium from basalt and andesite from surrounding volcanic arcs (Goddéris et al., 2017) during an interval of low relief and high continentality. The subsequent sharp rise of strontium isotope ratios from 0.85 Ga to the end of Precambrian encompasses the breakup of the supercontinent Rodinia at c.0.8-0.65 Ga (Condie and Puetz, 2019) and the assembly of Gondwana at c. 0.6-

828 0.5 Ga (Cawood and Buchan, 2007; Merdith et al., 2017). During breakup, the old and
829 radiogenic continental interiors might have been uplifted, exposed and rapidly
830 weathered, giving rise to an overall increase in ocean $^{87}Sr/^{86}Sr$, interrupted by several
831 eruptive events (Goddéris et al., 2017; Halverson et al., 2007; Zhou et al., 2020).
832 Simultaneously, the εHf and εNd curves start showing a decreasing trend, which
833 indicates that the crustal production began shifting to an advancing external phase,
834 where the reworked components with higher $^{87}Sr/^{86}Sr$ values exceeded juvenile
835 components with lower $^{87}Sr/^{86}Sr$ ratios (Condie and Aster, 2013). Afterwards, the
836 onset of Gondwana assembly produced widespread collisional orogens and generated
837 highly pulverised bedrocks by physical weathering, thereby promoting rapid
838 chemical weathering (Ruddiman et al., 1997). Abrupt increases in $^{87}Sr/^{86}Sr$ follow
839 both the Sturtian and Marinoan glaciations may relate to enhanced chemical
840 weathering of freshly exposed rock surfaces beneath a CO_2-rich atmosphere (e.g., Cox
841 et al., 2016). Such increases in weathering efficiency will eventually draw down
842 carbon dioxide levels, bringing weathering rates back down again. Alternatively,
843 Shields et al., (2019) proposed that a genuine rise of continental weathering rates
844 without lowering CO_2 if uplift and erosion events led to enhanced evaporite sulfate
845 weathering, which if coupled with pyrite burial/organic carbon oxidation could
846 maintain CO_2 forcing of chemical weathering. Continent-continent collisions might
847 also deliver the radiogenic isotope signal of the largely-reworked crust into the ocean,
848 given the sharp decreases in εHf and εNd as well as the rise of $\delta^{18}O$ values from c.
849 0.85 Ga to c. 0.55 Ga.

850 **8. Linking the updated Sr isotope record to supercontinental cycles**

851 Tectonic processes are the major influence on Sr fluxes to the ocean and the updated
852 seawater $^{87}Sr/^{86}Sr$ curve shows both stronger oscillations and better correspondence

853 with tectonic events than had previously been shown (Shields and Veizer, 2002) **(Fig.**
854 **5A; Fig. 6)**. In particular, supercontinent cycles, which have in the interim become
855 more evident in zircon abundance, s-type granite, metamorphic grade and zircon
856 isotopic records, show more convincing covariation with seawater $^{87}Sr/^{86}Sr$ throughout
857 the Proterozoic as well as the already established Phanerozoic Eon.

858 In the new curve, in most cases, rising $^{87}Sr/^{86}Sr$ rises coincide with proposed times
859 of supercontinent amalgamation; and $^{87}Sr/^{86}Sr$ falls accompany times of high
860 continentality / supercontinent tenure and initial breakup. For instance, the assembly
861 stages of supercontinent Kenorland (postulated), Nuna and Gondwana all correspond
862 to increases in the Sr isotope curve, while their tenure and rifting coincide with lower
863 points in the curve **(Fig. 5A).** It was suggested that supercontinent amalgamation
864 enhances continental weathering of uplifted terrains and increased input of radiogenic
865 Sr flux to the ocean, while supercontinent breakup is associated with ocean ridge
866 activity, rift-related magmatism and sea-level rise, leading to increased input of
867 relatively unradiogenic Sr flux to the ocean and low seawater $^{87}Sr/^{86}Sr$ values (e.g.,
868 Asmerom et al., 1991; Raymo et al., 1988; Veizer et al., 1989). It is worth noting that
869 the updated Sr isotope curve reaches peaks after zircon abundance peaks related to
870 supercontinent assembly. For example, for Nuna the Sr isotope peak at c. 1.7 Ga follows
871 a zircon abundance peak at c. 1.87 Ga and for Gondwana the c. 500 Ma acme follows
872 a peak at c. 600 Ma, which corresponds to rapid erosion of particularly high
873 “supermountains” as evidenced by the high production rate of S-type granites (Brown
874 and Johnson, 2019; Zhu et al., 2020). Orogeny may lead to higher seawater Sr isotope
875 ratio, not through chemical weathering, which is related to outgassing of carbon dioxide,
876 but to physical weathering, and desorption of Sr from fine-grained suspended sediment
877 carried by rivers, in which case Sr isotopes can act more as an erosional proxy than

878 merely chemical weathering (Oelkers et al., 2012). The extreme continental weathering
879 during assembly of Nuna and Gondwana may have triggered the increased input of bio-
880 essential materials to the ocean, fuelling the evolution and radiations of early eukaryotes
881 (late Paleoproterozoic; e.g., Javaux et al., 2018) and animals (Neoproterozoic-
882 Cambrian; e.g., Xiao and Laflamme, 2019), respectively **(Fig. 5D).**

883 One possible exception relates to the assembly and breakup of Rodinia and Pangaea.
884 Seawater $^{87}Sr/^{86}Sr$ values only experienced a modest increase during Rodinia
885 amalgamation and even a fall during Pangaea assembly, while their breakups were
886 associated with increases in the seawater Sr curve. Contrasting with the pronounced
887 negative εHf and εNd values during assembly of Nuna and Gondwana, Hf and Nd
888 isotope values are anomalously radiogenic (above the value of the chondritic uniform
889 reservoir) during the time of Rodinia and Pangaea amalgamation **(Fig. 5B)**, which
890 possibly indicates the predominant production and weathering of unradiogenic juvenile
891 crust (Condie and Aster, 2013; Spencer et al., 2013). Halverson et al., (2007) suggested
892 that supercontinent assembly might shift rainfall away from radiogenic continental
893 interiors to unradiogenic juvenile crust on the edges of continents, resulting in lower
894 seawater $^{87}Sr/^{86}Sr$; while supercontinental break-up could shift rainfall to older and
895 uplifted continental interiors, leading to an increase of seawater $^{87}Sr/^{86}Sr$. Therefore,
896 compared with other periods, during Rodinia and Pangaea assembly and breakup,
897 seawater Sr isotope values might be more controlled by compositional changes of Sr
898 sources undergoing weathering. Alternatively, Wang et al., (2021) presented the
899 concept of "megacontinent" as a geodynamic precursor and a large subset of the next
900 supercontinent. They suggested that the supercontinent Pangea was preceded by the
901 formation of "megacontinent" Gondwana that was formed by an assembly of multiple
902 continents and represented ~70% size of the Pangea. It is likely that supercontinent

amalgamation had less influence on global erosion rates than the preceding formation of its megacontinent, therefore resulting in the relatively low values of seawater Sr isotopes during Pangea amalgamation stage compared with the Gondwana assembly stage.

9. Conclusions

1) 2249 strontium isotope data points have been compiled from Precambrian marine carbonate rocks, from 62 publications and 3 unpublished materials over the past 18 years, and added to the previous seawater $^{87}Sr/^{86}Sr$ database by Shields and Veizer (2002). Four criteria (depositional environment, preservation, age constraints and dissolution methods) have been used to assign values to one of high, medium and low certainty groups.

2) After reviewing and summarizing diagenetic screening methods, a dynamic approach that generally includes field and petrological examinations, geochemical screening (major and trace elements, stable isotopes, and strontium isotopes) and coeval sample comparisons is recommended.

3) A range of analytical methods have been compared. In conclusion, pre-leaching of samples is essential because it removes Sr contamination from clay-associated ions and secondary carbonate overgrowths, thus enhancing the reliability of obtained values and potentially lessen the need for major Rb-decay correction. Aggressive acid leaching should be avoided as it attacks clay minerals in the rock matrix, thus contaminating original carbonate strontium isotope values.

4) An updated strontium isotope curve of Precambrian seawater has been generated based mainly on high-certainty data from the updated compilation. Compared with the previous version (Shields and Veizer, 2002), this updated curve exhibits relatively high-amplitude fluctuations that correspond to proposed

928 supercontinental cycles (wherein $^{87}Sr/^{86}Sr$ rises accompany supercontinent
929 amalgamation; and $^{87}Sr/^{86}Sr$ falls accompany supercontinent breakup).
930 5) Several hypotheses have been proposed based on the improved Sr isotope
931 curve. For instance, an earlier deflection of seawater $^{87}Sr/^{86}Sr$ from the
932 contemporaneous mantle at ~3.5 Ga might support the earlier onset of plate tectonics.
933 Two sharp rises in the new curve at 2.5-2.2 Ga and 1.9-1.7 Ga, with uncertainties,
934 indicate elevated continental weathering before and during the Great Oxygenation
935 Event and the assembly of supercontinent Nuna, respectively.
936 6) Significant data gaps still exist in the Neoarchean, late Paleoproterozoic and
937 Mesoproterozoic, requiring further work. More high-certainty data are needed to test
938 the hypotheses proposed in this study, especially during the periods of 2.5-2.2 Ga and
939 1.9-1.7 Ga.

940 **Acknowledgements**

941 The authors wish to thank Linda C. Kah, Galen Halverson, and A.B. Kuznetsov for
942 comments which have greatly improved the manuscript. The authors gratefully
943 acknowledge funding support from NERC grant NE/P013643/1 (BETR programme)
944 and Dean's Prize of the Faculty of Mathematical and Physical Sciences, UCL. We
945 also wish to thank J. McArthur for the helpful discussions and suggestions.

Appendix A: Supplementary data

Supplementary material 1. Precambrian strontium isotope database version 2021 (a).

Supplementary material 2. Precambrian strontium isotope database version 2021 (b).

Supplementary material 3: Reference lists for Precambrian strontium isotope database version 2021 (a).

References

Adam, Z.R., Skidmore, M.L., Mogk, D.W., Butterfield, N.J., 2017. A Laurentian record of the earliest fossil eukaryotes. Geology 45. https://doi.org/10.1130/G38749.1

Albarède, F., Michard, A., Minster, J.F., Michard, G., 1981. 87Sr86Sr ratios in hydrothermal waters and deposits from the East Pacific Rise at 21°N. Earth Planet. Sci. Lett. https://doi.org/10.1016/0012-821X(81)90102-3

Allègre, C.J., Louvat, P., Gaillardet, J., Meynadier, L., Rad, S., Capmas, F., 2010. The fundamental role of island arc weathering in the oceanic Sr isotope budget. Earth Planet. Sci. Lett. https://doi.org/10.1016/j.epsl.2010.01.019

Alvarenga, C.J.S., Oliveira, G.D., Vieira, L.C., Santos, R. V., Baptista, M.C., Dantas, E.L., 2019. Carbonate chemostratigraphy of the Vazante Group, Brazil: A probable Tonian age. Precambrian Res. 331, 105378. https://doi.org/10.1016/j.precamres.2019.105378

Alvarenga, C.J.S., Santos, R. V., Vieira, L.C., Lima, B.A.F., Mancini, L.H., 2014. Meso-Neoproterozoic isotope stratigraphy on carbonates platforms in the brasilia belt of Brazil. Precambrian Res. 251, 164–180. https://doi.org/10.1016/j.precamres.2014.06.011

Anderson, J.L. and Medaris, L.G., 1983. Proterozoic anorogenic granite plutonism of North America. Geol. Soc. Lond. Mem. 161, 133-154. https://doi.org/10.1130/MEM161-p133

Anderson, S.P., 2007. Biogeochemistry of glacial landscape systems. Annu. Rev. Earth Planet. Sci. 35. https://doi.org/10.1146/annurev.earth.35.031306.140033

973 Anderson, T.F., Arthur, M.A., 1983. Stable isotopes of oxygen and carbon and their
974 application to sedimentologic and paleoenvironmental problems. Stable Isot.
975 Sediment. Geol.

976 Asmerom, Y., Jacobsen, S.B., Knoll, A.H., Butterfield, N.J., Swett, K., 1991. Strontium
977 isotopic variations of Neoproterozoic seawater: Implications for crustal evolution.
978 Geochim. Cosmochim. Acta 55, 2883–2894. https://doi.org/10.1016/0016-
979 7037(91)90453-C

980 Aspler, L.B., Chiarenzelli, J.R., 1998. Two Neoarchean Supercontinents? Evidence
981 from the Paleoproterozoic. Sediment. Geol. 120, 75–104.
982 https://doi.org/10.1016/S0037- 0738(98)00028-1.

983 Azmy, K., Kaufman, A.J., Misi, A., Oliveira, T.F. de, 2006. Isotope stratigraphy of the
984 Lapa Formation, São Francisco Basin, Brazil: Implications for Late
985 Neoproterozoic glacial events in South America. Precambrian Res. 149, 231–248.
986 https://doi.org/10.1016/j.precamres.2006.07.001

987 Bachan, A., Kump, L.R., 2015. The rise of oxygen and siderite oxidation during the
988 Lomagundi event. Natl. Acad. Sci. U. S. A. 112, 6562–6567. https://doi.org/
989 10.1073/pnas.1422319112. Bailey, T.R., McArthur, J.M., Prince.

990 Bailey, T.R., McArthur, J.M., Prince, H., Thirlwall, M.F., 2000. Dissolution methods
991 for strontium isotope stratigraphy: Whole rock analysis. Chem. Geol. 167, 313–
992 319. https://doi.org/10.1016/S0009-2541(99)00235-1

993 Baker, A.J., Fallick, A.E., 1989. Evidence from Lewisian limestones for isotopically
994 heavy carbon in two-thousand-million-year-old sea water. Nature 337.
995 https://doi.org/10.1038/337352a0

996 Banner, J.L., 2004. Radiogenic isotopes: Systematics and applications to earth surface
997 processes and chemical stratigraphy. Earth-Science Rev.
998 https://doi.org/10.1016/S0012-8252(03)00086-2

999 Banner, J.L., 1995. Application of the trace element and isotope geochemistry of
1000 strontium to studies of carbonate diagenesis. Sedimentology.
1001 https://doi.org/10.1111/j.1365-3091.1995.tb00410.x

1002 Banner, J.L., Hanson, G.N., 1990. Calculation of simultaneous isotopic and trace
1003 element variations during water-rock interaction with applications to carbonate
1004 diagenesis. Geochim. Cosmochim. Acta. https://doi.org/10.1016/0016-
1005 7037(90)90128-8

1006 Barley, M.E., Bekker, A., Krapež, B., 2005. Late Archean to Early Paleoproterozoic
1007 global tectonics, environmental change and the rise of atmospheric oxygen. Earth
1008 Planet. Sci. Lett. https://doi.org/10.1016/j.epsl.2005.06.062

1009 Bartley, J.K., Kah, L.C., 2004. Marine carbon reservoir, Corg-Ccarb coupling, and the
1010 evolution of the Proterozoic carbon cycle. Geology 32.
1011 https://doi.org/10.1130/G19939.1

1012 Bartley, J.K., Kah, L.C., McWilliams, J.L., Stagner, A.F., 2007. Carbon isotope
1013 chemostratigraphy of the Middle Riphean type section (Avzyan Formation,
1014 Southern Urals, Russia): Signal recovery in a fold-and-thrust belt. Chem. Geol.
1015 237, 211–232. https://doi.org/10.1016/j.chemgeo.2006.06.018

1016 Bartley, J.K., Semikhatov, M.A., Kaufman, A.J., Knoll, A.H., Pope, M.C., Jacobsen,
1017 S.B., 2001. Global events across the Mesoproterozoic-Neoproterozoic boundary:
1018 C and Sr isotopic evidence from Siberia. Precambrian Res. 111, 165–202.

https://doi.org/10.1016/S0301-9268(01)00160-7

Bataille, C.P., Willis, A., Yang, X., Liu, X., 2017. Continental igneous rock composition: A major control of past global chemical weathering continental crust to seawater and exerts a direct control on several bio- surfaces have been invoked to explain some more specific features in screened database gath. Sci. Adv. 3, 1–16. https://doi.org/e1602183

Bates, N.R., Brand, U., 1991. Environmental and physiological influences on isotopic and elemental compositions of brachiopod shell calcite: Implications for the isotopic evolution of Paleozoic oceans. Chem. Geol. https://doi.org/10.1016/S0009-2541(10)80018-X

Bekker, A., Holland, H.D., 2012. Oxygen overshoot and recovery during the early Paleoproterozoic. Earth Planet. Sci. Lett. 317–318, 295–304. https://doi.org/10.1016/j.epsl.2011.12.012

Bekker, A., Holland, H.D., Wang, P.L., Rumble, D., Stein, H.J., Hannah, J.L., Coetzee, L.L., Beukes, N.J., 2004. Dating the rise of atmospheric oxygen. Nature. https://doi.org/10.1038/nature02260

Bekker, A., Karhu, J.A., Eriksson, K.A., Kaufman, A.J., 2003a. Chemostratigraphy of Paleoproterozoic carbonate successions of the Wyoming Craton: Tectonic forcing of biogeochemical change?, Precambrian Research. https://doi.org/10.1016/S0301-9268(02)00164-X

Bekker, A., Krapež, B., Müller, S.G., Karhu, J.A., 2016. A short-term, post-Lomagundi positive C isotope excursion at c. 2.03Ga recorded by the Wooly Dolomite, Western Australia. Journal of the Geological Society 173.

https://doi.org/10.1144/jgs2015- 152.

Bekker, A., Karhu, J.A., Kaufman, A.J., 2006. Carbon isotope record for the onset of the Lomagundi carbon isotope excursion in the Great Lakes area, North America. Precambrian Res. 148, 145–180. https://doi.org/10.1016/j.precamres.2006.03.008

Bekker, A., Kaufman, A.J., Karhu, J.A., Beukes, N.J., Swart, Q.D., Coetzee, L.L., Eriksson, K.A., 2001. Chemostratigraphy of the Paleoproterozoic Duitschland Formation, South Africa: Implications for coupled climate change and carbon cycling. Am. J. Sci. 301, 261–285. https://doi.org/10.2475/ajs.301.3.261

Bekker, A., Sial, A.N., Karhu, J.A., Ferreira, V.P., Noce, C.M., Kaufman, A.J., Romano, A.W., Pimentel, M.M., 2003b. Chemostratigraphy of carbonates from the Minas Supergroup, quadrilátero ferrífero (iron quadrangle), Brazil: A stratigraphic record of early proterozoic atmospheric, biogeochemical and climatic change. Am. J. Sci. https://doi.org/10.2475/ajs.303.10.865

Bellefroid, E.J., Hood, A.V.S., Hoffman, P.F., Thomas, M.D., Reinhard, C.T., Planavsky, N.J., 2018a. Constraints on paleoproterozoic atmospheric oxygen levels. Proc. Natl. Acad. Sci. U. S. A. 115, 8104–8109. https://doi.org/10.1073/pnas.1806216115

Bellefroid, E.J., Planavsky, N.J., Miller, N.R., Brand, U., Wang, C., 2018b. Case studies on the utility of sequential carbonate leaching for radiogenic strontium isotope analysis. Chem. Geol. 497, 88–99. https://doi.org/10.1016/j.chemgeo.2018.08.025

Belousova, E.A., Kostitsyn, Y.A., Griffin, W.L., Begg, G.C., O'Reilly, S.Y., Pearson, N.J., 2010. The growth of the continental crust: Constraints from zircon Hf-isotope data. Lithos 119, 457–466. https://doi.org/10.1016/j.lithos.2010.07.024

1065 Berner, R.A., 2003. The long-term carbon cycle, fossil fuels and atmospheric
1066 composition. Nature. https://doi.org/10.1038/nature02131

1067 Berner, R.A., Lasaga, A.C., Garrels, R.M., 1983. The carbonate-silicate geochemical
1068 cycle and its effect on atmospheric carbon dioxide over the past 100 million years.
1069 Am. J. Sci. https://doi.org/10.2475/ajs.283.7.641

1070 Bleeker, W., 2003. The late Archean record: A puzzle in ca. 35 pieces. Lithos.
1071 https://doi.org/10.1016/j.lithos.2003.07.003

1072 Bold, U., Smith, E.F., Rooney, A.D., Bowring, S.A., Buchwaldt, R., Dudás, F.O.,
1073 Ramezani, J., Crowley, J.L., Schrag, D.P., Macdonald, F.A., 2016. Neoproterozoic
1074 stratigraphy of the zavkhan terrane of Mongolia: The backbone for cryogenian and
1075 early ediacaran chemostratigraphic records. Am. J. Sci. 315, 1–63.
1076 https://doi.org/10.2475/01.2016.01

1077 Bowen, G.J., Wilkinson, B., 2002. Spatial distribution of δ18O in meteoric precipitation.
1078 Geology 30. https://doi.org/10.1130/0091-
1079 7613(2002)030<0315:SDOOIM>2.0.CO;2

1080 Bradley, D.C., 2011. Secular trends in the geologic record and the supercontinent cycle.
1081 Earth-Science Rev. 108, 16–33. https://doi.org/10.1016/j.earscirev.2011.05.003

1082 Bradley, D.C., 2008. Passive margins through earth history. Earth-Science Rev. 91, 1–
1083 26. https://doi.org/10.1016/j.earscirev.2008.08.001

1084 Brand, U., 2004. Carbon, oxygen and strontium isotopes in Paleozoic carbonate
1085 components: An evaluation of original seawater-chemistry proxies. Chem. Geol.
1086 https://doi.org/10.1016/j.chemgeo.2003.10.013

1087 Brand, U., Azmy, K., Tazawa, J.I., Sano, H., Buhl, D., 2010. Hydrothermal diagenesis
1088 of Paleozoic seamount carbonate components. Chem. Geol.
1089 https://doi.org/10.1016/j.chemgeo.2010.09.010

1090 Brand, U., Brenckle, P., 2001. Chemostratigraphy of the Mid-Carboniferous boundary
1091 global stratotype section and point (GSSP), Bird Spring Formation, Arrow Canyon,
1092 Nevada, USA. Palaeogeogr. Palaeoclimatol. Palaeoecol.
1093 https://doi.org/10.1016/S0031-0182(00)00169-3

1094 Brand, U., Jiang, G., Azmy, K., Bishop, J., Montañez, I.P., 2012. Diagenetic evaluation
1095 of a Pennsylvanian carbonate succession (Bird Spring Formation, Arrow Canyon,
1096 Nevada, U.S.A.) - 1: Brachiopod and whole rock comparison. Chem. Geol.
1097 https://doi.org/10.1016/j.chemgeo.2012.03.017

1098 Brand, U., Veizer, J., 1981. Chemical diagenesis of a multicomponent carbonate system
1099 - 2: stable isotopes. J. Sediment. Petrol. https://doi.org/10.1306/212F7DF6-2B24-
1100 11D7-8648000102C1865D

1101 Brand, U., Veizer, J., 1980. Chemical diagenesis of a multicomponent carbonate system
1102 - 1. Trace elements. J. Sediment. Petrol. https://doi.org/10.1306/212F7BB7-2B24-
1103 11D7-8648000102C1865D

1104 Brasier, M.D., Lindsay, J.F., 1998. A billion years of environmental stability and the
1105 emergence of eukaryotes: new data from northern Australia. Geology 26.
1106 https://doi.org/10.1130/0091-7613(1998)026<0555:ABYOES>2.3.CO;2

1107 Brass, G.W., 1976. The variation of the marine 87Sr86Sr ratio during Phanerozonic
1108 time: interpretation using a flux model. Geochim. Cosmochim. Acta.
1109 https://doi.org/10.1016/0016-7037(76)90025-9

Broecker, W.S., Peng, T.H., 1983. Tracers in the Sea. https://doi.org/10.1016/0016-7037(83)90075-3

Brown, M., Johnson, T., 2019. Metamorphism and the evolution of subduction on Earth. Am. Mineral. 104. https://doi.org/10.2138/am-2019-6956

Brown, M., Johnson, T., Gardiner, N.J., 2020. Plate Tectonics and the Archean Earth. Annu. Rev. Earth Planet. Sci. 48, 291–320. https://doi.org/10.1146/annurev-earth-081619-052705

Bruland, K.W., Middag, R., Lohan, M.C., 2014. 8.2 - Controls of Trace Metals in Seawater A2 - Holland, Heinrich D, in: Treatise on Geochemistry (Second Edition). https://doi.org/https://doi.org/10.1016/B978-0-08-095975-7.00602-1

Bryan, S.E., Ernst, R.E., 2008. Revised definition of Large Igneous Provinces (LIPs). Earth-Science Rev. 86. https://doi.org/10.1016/j.earscirev.2007.08.008

Buick, R., Des Marais, D.J., Knoll, A.H., 1995. Stable isotopic compositions of carbonates from the Mesoproterozoic Bangemall group, northwestern Australia. Chem. Geol. https://doi.org/10.1016/0009-2541(95)00049-R

Burke, W.H., Denison, R.E., Hetherington, E.A., Koepnick, R.B., Nelson, H.F., Otto, J.B., 1982. Variation of seawater 87 Sr/ 86 Sr throughout Phanerozoic time. Geology. https://doi.org/10.1130/0091-7613(1982)10<516:VOSSTP>2.0.CO;2

Butterfield, N.J., 2000. Bangiomorpha pubescens n. gen., n. sp.: implications for the evolution of sex, multicellularity, and the Mesoproterozoic/Neoproterozoic radiation of eukaryotes . Paleobiology. https://doi.org/10.1666/0094-8373(2000)026<0386:bpngns>2.0.co;2

1132 Butterfield, N.J., Knoll, A.H., Swett, K., 1990. A bangiophyte red alga from the
1133 proterozoic of arctic Canada. Science. 250.
1134 https://doi.org/10.1126/science.11538072

1135 Canfield, D.E., Ngombi-Pemba, L., Hammarlund, E.U., Bengtson, S., Chaussidon, M.,
1136 Gauthier-Lafaye, F., Meunier, A., Riboulleau, A., Rollion-Bard, C., Rouxel, O.,
1137 Asael, D., Pierson-Wickmann, A.C., El Albani, A., 2013. Oxygen dynamics in the
1138 aftermath of the Great Oxidation of Earth's atmosphere. Proc. Natl. Acad. Sci. U.
1139 S. A. 110. https://doi.org/10.1073/pnas.1315570110

1140 Canfield, D.E., Thamdrup, B., 2009. Towards a consistent classification scheme for
1141 geochemical environments, or, why we wish the term "suboxic" would go away:
1142 Editorial. Geobiology. https://doi.org/10.1111/j.1472-4669.2009.00214.x

1143 Catling, D.C., Zahnle, K.J., 2020. The Archean atmosphere. Sci. Adv. 6.
1144 https://doi.org/10.1126/sciadv.aax1420

1145 Cawood, P.A., 2020. Earth Matters : A tempo to our planet ' s evolution 48, 525–526.

1146 Cawood, P.A., Buchan, C., 2007. Linking accretionary orogenesis with supercontinent
1147 assembly. Earth-Science Rev. https://doi.org/10.1016/j.earscirev.2007.03.003

1148 Cawood, P.A., Hawkesworth, C.J., 2014. Earth's middle age. Geology 42, 503–506.
1149 https://doi.org/10.1130/G35402.1

1150 Cawood, P.A., Hawkesworth, C.J., Dhuime, B., 2013. The continental record and the
1151 generation of continental crust. Bull. Geol. Soc. Am. 125.
1152 https://doi.org/10.1130/B30722.1

1153 Cawood, P.A., Hawkesworth, C.J., Pisarevsky, S.A., Dhuime, B., Capitanio, F.A.,

Nebel, O., 2018. Geological archive of the onset of plate tectonics. Philos. Trans. R. Soc. A Math. Phys. Eng. Sci. 376. https://doi.org/10.1098/rsta.2017.0405

Cawood, P.A., Kröner, A., Pisarevsky, S., 2006. Precambrian plate tectonics: Criteria and evidence. GSA Today 16. https://doi.org/10.1130/GSAT01607.1

Clayton, R.N., Epstein, S., 1958. The Relationship between O18/O16 Ratios in Coexisting Quartz, Carbonate, and Iron Oxides from Various Geological Deposits. J. Geol. https://doi.org/10.1086/626523

Coffin, M.F., Eldholm, O., 1994. Large igneous provinces: Crustal structure, dimensions, and external consequences. Rev. Geophys. https://doi.org/10.1029/93RG02508

Collins, W.J., Belousova, E.A., Kemp, A.I.S., Murphy, J.B., 2011. Two contrasting Phanerozoic orogenic systems revealed by hafnium isotope data. Nat. Geosci. 4, 333–337. https://doi.org/10.1038/ngeo1127

Condie, K.C., 2014. Growth of continental crust: a balance between preservation and recycling. Mineral. Mag. 78, 623–637. https://doi.org/10.1180/minmag.2014.078.3.11

Condie, K.C., 2004. Supercontinents and superplume events: Distinguishing signals in the geologic record. Phys. Earth Planet. Inter. 146. https://doi.org/10.1016/j.pepi.2003.04.002

Condie, K.C., n.d. Revisiting the Mesoproterozoic. Gondwana Res. https://doi.org/10.1016/j.gr.2020.08.001

Condie, K.C., Aster, R.C., 2013. Refinement of the supercontinent cycle with Hf, Nd

1176 and Sr isotopes. Geosci. Front. 4, 667–680.
1177 https://doi.org/10.1016/j.gsf.2013.06.001

1178 Condie, K.C., Bickford, M.E., Aster, R.C., Belousova, E., Scholl, D.W., 2011. Episodic
1179 zircon ages, Hf isotopic composition, and the preservation rate of continental crust.
1180 Bull. Geol. Soc. Am. 123. https://doi.org/10.1130/B30344.1

1181 Condie, K.C., Puetz, S.J., 2019. Time series analysis of mantle cycles Part II: The
1182 geologic record in zircons, large igneous provinces and mantle lithosphere. Geosci.
1183 Front. 10, 1327–1336. https://doi.org/10.1016/j.gsf.2019.03.005

1184 Corliss, J.B., Dymond, J., Gordon, L.I., Edmond, J.M., Von Herzen, R.P., Ballard, R.D.,
1185 Green, K., Williams, D., Bainbridge, A., Crane, K., Van Andel, T.H., 1979.
1186 Submarine thermal springs on the Galápagos Rift. Science (80-.).
1187 https://doi.org/10.1126/science.203.4385.1073

1188 Cox, G.M., Halverson, G.P., Stevenson, R.K., Vokaty, M., Poirier, A., Kunzmann, M.,
1189 Li, Z.X., Denyszyn, S.W., Strauss, J. V., Macdonald, F.A., 2016. Continental flood
1190 basalt weathering as a trigger for Neoproterozoic Snowball Earth. Earth Planet.
1191 Sci. Lett. 446, 89–99. https://doi.org/10.1016/j.epsl.2016.04.016

1192 Cui, H., Kaufman, A.J., Xiao, S., Zhu, M., Zhou, C., Liu, X.M., 2015. Redox
1193 architecture of an Ediacaran ocean margin: Integrated chemostratigraphic (δ13C-
1194 δ34S-87Sr/86Sr-Ce/Ce*) correlation of the Doushantuo Formation, South China.
1195 Chem. Geol. 405, 48–62. https://doi.org/10.1016/j.chemgeo.2015.04.009

1196 Cui, H., Kaufman, A.J., Zou, H., Kattan, F.H., Trusler, P., Smith, J., Yu. Ivantsov, A.,
1197 Rich, T.H., Al Qubsani, A., Yazedi, A., Liu, X.M., Johnson, P., Goderis, S., Claeys,
1198 P., Vickers-Rich, P., 2020. Primary or secondary? A dichotomy of the strontium

1199 isotope anomalies in the Ediacaran carbonates of Saudi Arabia. Precambrian Res.
1200 343, 105720. https://doi.org/10.1016/j.precamres.2020.105720

1201 Daly, J.S., Balagansky, V. V., Timmerman, M.J., Whitehouse, M.J., 2006. The
1202 Lapland-Kola orogen: Palaeoproterozoic collision and accretion of the northern
1203 Fennoscandian lithosphere. Geol. Soc. Mem.
1204 https://doi.org/10.1144/GSL.MEM.2006.032.01.35

1205 Degens, E.T., Epstein, S., 1964. Oxygen and carbon isotope ratios in coexisting calcites
1206 and dolomites from recent and ancient sediments. Geochim. Cosmochim. Acta.
1207 https://doi.org/10.1016/0016-7037(64)90053-5

1208 Denison, R.E., Koepnick, R.B., Fletcher, A., Howell, M.W., Callaway, W.S., 1994.
1209 Criteria for the retention of original seawater 87Sr86Sr in ancient shelf limestones.
1210 Chem. Geol. https://doi.org/10.1016/0009-2541(94)90110-4

1211 Derry, L.A., Kaufman, A.J., Jacobsen, S.B., 1992. Sedimentary cycling and
1212 environmental change in the Late Proterozoic: Evidence from stable and
1213 radiogenic isotopes. Geochim. Cosmochim. Acta 56, 1317–1329.
1214 https://doi.org/10.1016/0016-7037(92)90064-P

1215 Dessert, C., Dupré, B., François, L.M., Schott, J., Gaillardet, J., Chakrapani, G., Bajpai,
1216 S., 2001. Erosion of Deccan Traps determined by river geochemistry: Impact on
1217 the global climate and the 87Sr/86Sr ratio of seawater. Earth Planet. Sci. Lett. 188.
1218 https://doi.org/10.1016/S0012-821X(01)00317-X

1219 Dhuime, B., Hawkesworth, C.J., Cawood, P.A., Storey, C.D., 2012. A change in the
1220 geodynamics of continental growth 3 billion years ago. Science (80-.).
1221 https://doi.org/10.1126/science.1216066

Dhuime, B., Wuestefeld, A., Hawkesworth, C.J., 2015. Emergence of modern continental crust about 3 billion years ago. Nat. Geosci. 8, 552–555. https://doi.org/10.1038/ngeo2466

Diamond, C.W., Planavsky, N.J., Wang, C., Lyons, T.W., 2018. What the ~1.4 Ga Xiamaling Formation can and cannot tell us about the mid-Proterozoic ocean. Geobiology 16, 219–236. https://doi.org/10.1111/gbi.12282

Eiler, J.M., 2001. Oxygen isotope variations of basaltic lavas and upper mantle rocks. Rev. Mineral. Geochemistry 43. https://doi.org/10.2138/gsrmg.43.1.319

Elderfield, H., 1986. Strontium isotope stratigraphy. Palaeogeogr. Palaeoclimatol. Palaeoecol. https://doi.org/10.1016/0031-0182(86)90007-6

Elias, S., Ruddiman, W.F., 2000. Tectonic Uplift and Climate Change. Arctic, Antarct. Alp. Res. https://doi.org/10.2307/1552459

Eme, L., Sharpe, S.C., Brown, M.W., Roger, A.J., 2014. On the Age of Eukaryotes: Evaluating Evidence from Fossils and Molecular Clocks. Cold Spring Harb. Perspect. Biol. 6. https://doi.org/10.1101/cshperspect.a016139

Ernst, R.E., Ernst, R.E., 2014. Introduction, definition, and general characteristics, Large Igneous Provinces. https://doi.org/10.1017/cbo9781139025300.001

Ernst, R.E., Youbi, N., 2017. How Large Igneous Provinces affect global climate, sometimes cause mass extinctions, and represent natural markers in the geological record. Palaeogeogr. Palaeoclimatol. Palaeoecol. 478, 30–52. https://doi.org/10.1016/j.palaeo.2017.03.014

Ernst, W.G., Sleep, N.H., Tsujimori, T., 2016. Plate-tectonic evolution of the earth:

Bottom-up and top-down mantle circulation. Can. J. Earth Sci. 53. https://doi.org/10.1139/cjes-2015-0126

Evans, D.A.D., Mitchell, R.N., 2011. Assembly and breakup of the core of Paleoproterozoic-Mesoproterozoic supercontinent Nuna. Geology 39, 443–446. https://doi.org/10.1130/G31654.1

Fairchild, I.J., Einsele, G., Song, T., 1997. Possible seismic origin of molar tooth structures in Neoproterozoic carbonate ramp deposits, north China. Sedimentology 44. https://doi.org/10.1046/j.1365-3091.1997.d01-40.x

Fairchild, I.J., Spencer, A.M., Ali, D.O., Anderson, R.P., Anderton, R., Boomer, I., Dove, D., Evans, J.D., Hambrey, M.J., Howe, J., Sawaki, Y., Shields, G.A., Skelton, A., Tucker, M.E., Wang, Z., Zhou, Y., 2018. Tonian-Cryogenian boundary sections of Argyll, Scotland. Precambrian Res. 319, 37–64. https://doi.org/10.1016/j.precamres.2017.09.020

Faure, G., Hurley, P.M., Powell, J.L., 1965. The isotopic composition of strontium in surface water from the North Atlantic Ocean. Geochim. Cosmochim. Acta. https://doi.org/10.1016/0016-7037(65)90018-9

Flament, N., Coltice, N., Rey, P.F., 2013. The evolution of the 87sr/86sr of marine carbonates does not constrain continental growth. Precambrian Res. 229, 177–188. https://doi.org/10.1016/j.precamres.2011.10.009

Frank, T.D., Kah, L.C., Lyons, T.W., 2003. Changes in organic matter production and accumulation as a mechanism for isotopic evolution in the Mesoproterozoic ocean. Geol. Mag. 140. https://doi.org/10.1017/S0016756803007830

Frauenstein, F., Veizer, J., Beukes, N., Van Niekerk, H.S., Coetzee, L.L., 2009. Transvaal Supergroup carbonates: Implications for Paleoproterozoic δ18O and δ13C records. Precambrian Res. 175, 149–160. https://doi.org/10.1016/j.precamres.2009.09.005

Furniss, G., Rittel, J.F., Winston, D., 1998. Gas bubble and expansion crack origin of "Molar-tooth" calcite structures in the Middle Proterozoic Belt Supergroup, Western Montana. J. Sediment. Res. 68. https://doi.org/10.2110/jsr.68.104

Galindo, C., Casquet, C., Rapela, C., Pankhurst, R.J., Baldo, E., Saavedra, J., 2004. Sr, C and O isotope geochemistry and stratigraphy of Precambrian and lower Paleozoic carbonate sequences from the Western Sierras Pampeanas of Argentina: Tectonic implications. Precambrian Res. 131, 55–71. https://doi.org/10.1016/j.precamres.2003.12.007

Galy, A., France-Lanord, C., 1999. The strontium isotopic budget of Himalayan rivers in Nepal and Bangladesh. Geochim. Cosmochim. Acta.

George, B.G., Ray, J.S., Kumar, S., 2019. Geochemistry of carbonate formations of the chhattisgarh supergroup, central india: Implications for mesoproterozoic global events. Can. J. Earth Sci. 56, 335–346. https://doi.org/10.1139/cjes-2018-0144

Gernon, T.M., Hincks, T.K., Tyrrell, T., Rohling, E.J. and Palmer, M.R., 2016. Snowball Earth ocean chemistry driven by extensive ridge volcanism during Rodinia breakup. Nature Geosci. 9, 242–248. https://doi.org/10.1038/ngeo2632

Gibson, T.M., Wörndle, S., Crockford, P.W., Bui, T.H., Creaser, R.A., Halverson, G.P., 2019. Radiogenic isotope chemostratigraphy reveals marine and nonmarine depositional environments in the late Mesoproterozoic Borden Basin, Arctic

Canada. GSA Bull. 1965–1978. https://doi.org/10.1130/b35060.1

Gilleaudeau, G.J., Kah, L.C., 2015. Heterogeneous redox conditions and a shallow chemocline in the Mesoproterozoic ocean: Evidence from carbon-sulfur-iron relationships. Precambrian Res. 257, 94–108. https://doi.org/10.1016/j.precamres.2014.11.030

Gilleaudeau, G.J., Kah, L.C., 2013. Carbon isotope records in a Mesoproterozoic epicratonic sea: Carbon cycling in a low-oxygen world. Precambrian Res. 228. https://doi.org/10.1016/j.precamres.2013.01.006

Gilleaudeau, G.J., Sahoo, S.K., Kah, L.C., Henderson, M.A., Kaufman, A.J., 2018. Proterozoic carbonates of the Vindhyan Basin, India: Chemostratigraphy and diagenesis. Gondwana Res. 57. https://doi.org/10.1016/j.gr.2018.01.003

Goddéris, Y., Donnadieu, Y., Nédélec, A., Dupré, B., Dessert, C., Grard, A., Ramstein, G. and François, L.M., 2003. The Sturtian 'snowball'glaciation: fire and ice. Earth and Planetary Science Letters, 211(1-2), 1-12. https://doi.org/10.1016/S0012-821X(03)00197-3

Goddéris, Y., Le Hir, G., Macouin, M., Donnadieu, Y., Hubert-Théou, L., Dera, G., Aretz, M., Fluteau, F., Li, Z.X., Halverson, G.P., 2017. Paleogeographic forcing of the strontium isotopic cycle in the Neoproterozoic. Gondwana Res. 42, 151–162. https://doi.org/10.1016/j.gr.2016.09.013

Goldstein, S.J., Jacobsen, S.B., 1987. The Nd and Sr isotopic systematics of river-water dissolved material: Implications for the sources of Nd and Sr in seawater. Chem. Geol. Isot. Geosci. Sect. https://doi.org/10.1016/0168-9622(87)90045-5

1311 Gorokhov, I., Semikhatov, M., Baskakov, A., Kutyavin, E., Mel'Nikov, N., Sochava,
1312 A., Turchenko, T., 1995. Sr isotopic composition in Riphean, Vendian, and Lower
1313 Cambrian carbonates from Siberia. Stratigr. Geol. Correl. 3, 1–28.

1314 Greber, N.D., Dauphas, N., Bekker, A., Ptáček, M.P., Bindeman, I.N., Hofmann, A.,
1315 2017. Titanium isotopic evidence for felsic crust and plate tectonics 3.5 billion
1316 years ago. Science (80-.). 357. https://doi.org/10.1126/science.aan8086

1317 Griffin, W.L., Belousova, E.A., O'Neill, C., O'Reilly, S.Y., Malkovets, V., Pearson,
1318 N.J., Spetsius, S., Wilde, S.A., 2014. The world turns over: Hadean-Archean crust-
1319 mantle evolution. Lithos. https://doi.org/10.1016/j.lithos.2013.08.018

1320 Griffith, E.M., Paytan, A., 2012. Barite in the ocean - occurrence, geochemistry and
1321 palaeoceanographic applications. Sedimentology 59.
1322 https://doi.org/10.1111/j.1365-3091.2012.01327.x

1323 Hall, S.M., Veizer, J., 1996. Geochemistry of Precambrian carbonates: VII. Belt
1324 supergroup, Montana and Idaho, USA. Geochim. Cosmochim. Acta.
1325 https://doi.org/10.1016/0016-7037(95)00424-6

1326 Hallet, B., Hunter, L., Bogen, J., 1996. Rates of erosion and sediment evacuation by
1327 glaciers: A review of field data and their implications. Glob. Planet. Change 12.
1328 https://doi.org/10.1016/0921-8181(95)00021-6

1329 Halverson, G.P., 2007. A Neoproterozoic Chronology. Neoproterozoic Geobiol.
1330 Paleobiol. 231–271. https://doi.org/10.1007/1-4020-5202-2_8

1331 Halverson, G.P., Dudás, F.Ö., Maloof, A.C., Bowring, S.A., 2007. Evolution of the
1332 87Sr/86Sr composition of Neoproterozoic seawater. Palaeogeogr. Palaeoclimatol.

1333 Palaeoecol. 256, 103–129. https://doi.org/10.1016/j.palaeo.2007.02.028

1334 Halverson, G.P., Hoffman, P.F., Schrag, D.P., Kaufman, A.J., 2002. A major
1335 perturbation of the carbon cycle before the Ghaub glaciation (Neoproterozoic) in
1336 Namibia: Prelude to snowball Earth? Geochemistry, Geophys. Geosystems 3, 1–
1337 24. https://doi.org/10.1029/2001gc000244

1338 Halverson, G.P., Hoffman, P.F., Schrag, D.P., Maloof, A.C., Rice, A.H.N., 2005.
1339 Toward a Neoproterozoic composite carbon-isotope record. Bull. Geol. Soc. Am.
1340 117, 1181–1207. https://doi.org/10.1130/B25630.1

1341 Halverson, G.P., Wade, B.P., Hurtgen, M.T., Barovich, K.M., 2010a. Neoproterozoic
1342 chemostratigraphy. Precambrian Res.
1343 https://doi.org/10.1016/j.precamres.2010.04.007

1344 Halverson, G.P., Wade, B.P., Hurtgen, M.T., Barovich, K.M., 2010b. Neoproterozoic
1345 chemostratigraphy. Precambrian Res. 182, 337–350.
1346 https://doi.org/10.1016/j.precamres.2010.04.007

1347 Harrison, T.M., Schmitt, A.K., McCulloch, M.T., Lovera, O.M., 2008. Early (≥ 4.5 Ga)
1348 formation of terrestrial crust: Lu-Hf, δ18O, and Ti thermometry results for Hadean
1349 zircons. Earth Planet. Sci. Lett. 268. https://doi.org/10.1016/j.epsl.2008.02.011

1350 Hawkesworth, C., Cawood, P., Kemp, T., Storey, C., Dhuime, B., 2009. Geochemistry:
1351 A matter of preservation. Science (80-.). https://doi.org/10.1126/science.1168549

1352 Hawkesworth, C.J., Cawood, P.A., Dhuime, B., 2020. The Evolution of the Continental
1353 Crust and the Onset of Plate Tectonics. Front. Earth Sci. 8, 1–23.
1354 https://doi.org/10.3389/feart.2020.00326

1355 Hawkesworth, C.J., Cawood, P.A., Dhuime, B., 2016. Tectonics and crustal evolution.
1356 GSA Today 26, 4–11. https://doi.org/10.1130/GSATG272A.1

1357 Hawkesworth, C.J., Cawood, P.A., Dhuime, B., Kemp, T.I.S., 2017. Earth's continental
1358 lithosphere through time. Annu. Rev. Earth Planet. Sci. 45.
1359 https://doi.org/10.1146/annurev-earth-063016-020525

1360 Hawkesworth, C.J., Dhuime, B., Pietranik, A.B., Cawood, P.A., Kemp, A.I.S., Storey,
1361 C.D., 2010. The generation and evolution of the continental crust. J. Geol. Soc.
1362 London. 167, 229–248. https://doi.org/10.1144/0016-76492009-072

1363 Hemming, N.G., Meyers, W.J., Grams, J.C., 1989. Cathodoluminescence in diagenetic
1364 calcites: the roles of Fe and Mn as deduced from electron probe and
1365 spectrophotometric measurements. J. Sediment. Petrol. 59.
1366 https://doi.org/10.1306/212f8fa8-2b24-11d7-8648000102c1865d

1367 Herman, F., Seward, D., Valla, P.G., Carter, A., Kohn, B., Willett, S.D., Ehlers, T.A.,
1368 2013. Worldwide acceleration of mountain erosion under a cooling climate.
1369 Nature 504. https://doi.org/10.1038/nature12877

1370 Hessler, A.M., Lowe, D.R., 2006. Weathering and sediment generation in the Archean:
1371 An integrated study of the evolution of siliciclastic sedimentary rocks of the 3.2
1372 Ga Moodies Group, Barberton Greenstone Belt, South Africa. Precambrian Res.
1373 151, 185–210. https://doi.org/10.1016/j.precamres.2006.08.008

1374 Higgins, J.A., Bla, C.L., Lundstrom, E.A., Santiago-ramos, D.P., Akhtar, A.A., Cru, A.,
1375 Bialik, O., Holmden, C., Bradbury, H., 2018. ScienceDirect Mineralogy , early
1376 marine diagenesis , and the chemistry of shallow-water carbonate sediments 220,
1377 512–534. https://doi.org/10.1016/j.gca.2017.09.046

Hodell, D.A., Mead, G.A., Mueller, P.A., 1990. Variation in the strontium isotopic composition of seawater (8 Ma to present) : Implications for chemical weathering rates and dissolved fluxes to the oceans. Chem. Geol. Isot. Geosci. Sect. https://doi.org/10.1016/0168-9622(90)90011-Z

Hofmann, H.J., 1999. Geons and geons. Geology. https://doi.org/10.1130/0091-7613(1999)027<0855:GAG>2.3.CO;2

Hofmann, H.J., 1976. Precambrian Microflora, Belcher Islands, Canada: Significance and Systematics. J. Paleontol. 50.

Hoffman, P.F., Abbot, D.S., Ashkenazy, Y., Benn, D.I., Brocks, J.J., Cohen, P.A., Cox, G. M., Creveling, J.R., Donnadieu, Y., Erwin, D.H., Fairchild, I.J., Ferreira, D., Goodman, J.C., Halverson, G.P., Jansen, M.F., Le Hir, G., Love, G.D., Macdonald, F. A., Maloof, A.C., Partin, C.A., Ramstein, G., Rose, B.E.J., Rose, C.V., Sadler, P.M., Tziperman, E., Voigt, A., Warren, S.G., 2017. Snowball Earth climate dynamics and Cryogenian geology-geobiology. Sci. Adv. 3 https://doi.org/10.1126/ sciadv.1600983.

Hoffman, P.F., Lamothe, K.G., 2019. Seawater-buffered diagenesis, destruction of carbon isotope excursions, and the composition of DIC in Neoproterozoic oceans. Proc. Natl. Acad. Sci. U. S. A 116, 18874–18879. https://doi.org/10.1073/pnas.1909570116. Hofmann, H.J., 1976. Precambrian Microflora, Belcher Islands, Canada: significance and systematics. J. Paleontol. 50.

Holland, H.D., 2002. Volcanic gases, black smokers, and the great oxidation event. Geochim. Cosmochim. Acta. https://doi.org/10.1016/S0016-7037(02)00950-X

1401 Hopkins, M., Harrison, T.M., Manning, C.E., 2008. Low heat flow inferred from >4
1402 Gyr zircons suggests Hadean plate boundary interactions. Nature 456.
1403 https://doi.org/10.1038/nature07465

1404 Huang, Z., Yuan, C., Long, X., Zhang, Y., Du, L., 2019. From Breakup of Nuna to
1405 Assembly of Rodinia: A Link Between the Chinese Central Tianshan Block and
1406 Fennoscandia. Tectonics. https://doi.org/10.1029/2018TC005471

1407 Jacobsen, S.B., Kaufman, A.J., 1999. The Sr, C and O isotopic evolution of
1408 Neoproterozoic seawater. Chem. Geol. https://doi.org/10.1016/S0009-
1409 2541(99)00080-7

1410 Jagoutz, O., Macdonald, F.A., Royden, L., 2016. Low-latitude arc-continent collision
1411 as a driver for global cooling. Proc. Natl. Acad. Sci. U. S. A. 113.
1412 https://doi.org/10.1073/pnas.1523667113

1413 James, N.P., Narbonne, G.M., Sherman, A.G., 1998. Molar-tooth carbonates: shallow
1414 subtidal facies of the mid- to late proterozoic. J. Sediment. Res. 68.
1415 https://doi.org/10.2110/jsr.68.716

1416 Javaux, E.J., Knoll, A.H., Walter, M.R., 2001. Morphological and ecological
1417 complexity in early eukaryotic ecosystems. Nature 412.
1418 https://doi.org/10.1038/35083562

1419 Javaux, E.J., Lepot, K., 2018. The Paleoproterozoic fossil record: Implications for the
1420 evolution of the biosphere during Earth's middle-age. Earth-Science Rev. 176, 68–
1421 86. https://doi.org/10.1016/j.earscirev.2017.10.001

1422 Javaux, E.J., Lepot, K., van Zuilen, M., Melezhik, V.A., Medvedev, P. V., 2013.

Palaeoproterozoic microfossils. Front. Earth Sci. 8.

Johnston, D.T., Wing, B.A., Farquhar, J., Kaufman, A.J., Strauss, H., Lyons, T.W., Kah, L.C., Canfield, D.E., 2005. Geochemistry: Active microbial sulfur disproportionation in the mesoproterozoic. Science (80-.). 310. https://doi.org/10.1126/science.1117824

Kah, L.C., 2000. Depositional d18O Signatures in Proterozoic Dolostones: Constraints on Seawater Chemistry and Early Diagenesis. SEPM Spec. Publ. 67.

Kah, L.C., Bartley, J.K., 2011. Protracted oxygenation of the Proterozoic biosphere. Int. Geol. Rev. 53, 1424–1442. https://doi.org/10.1080/00206814.2010.527651

Kah, L.C., Bartley, J.K., Teal, D.A., 2012. Chemostratigraphy of the Late Mesoproterozoic Atar Group, Taoudeni Basin, Mauritania: Muted isotopic variability, facies correlation, and global isotopic trends. Precambrian Res. 200–203, 82–103. https://doi.org/10.1016/j.precamres.2012.01.011

Kah, L.C., Lyons, T.W., Chesley, J.T., 2001. Geochemistry of a 1.2 Ga carbonate-evaporite succession, northern Baffin and Bylot Islands: Implications for Mesoproterozoic marine evolution. Precambrian Res. 111, 203–234. https://doi.org/10.1016/S0301-9268(01)00161-9

Kah, L.C., Lyons, T.W., Frank, T.D., 2004. Low marine sulphate and protracted oxygenation of the Proterozoic biosphere. Nature 431. https://doi.org/10.1038/nature02974

Kah, L.C., Sherman, A.G., Narbonne, G.M., Knoll, A.H., Kaufman, A.J., 1999. δ13C stratigraphy of the Proterozoic Bylot Supergroup, Baffin Island, Canada:

Implications for regional lithostratigraphic correlations. Can. J. Earth Sci. 36. https://doi.org/10.1139/e98-100

Kamber, B.S., Webb, G.E., 2001. The geochemistry of late Archaean microbial carbonate: Implications for ocean chemistry and continental erosion history. Geochim. Cosmochim. Acta 65, 2509–2525. https://doi.org/10.1016/S0016-7037(01)00613-5

Karhu, J.A., Holland, H.D., 1996. Carbon isotopes and the rise of atmospheric oxygen. Geology 24. https://doi.org/10.1130/0091-7613(1996)024<0867:CIATRO>2.3.CO;2

Kaufman, A.J., Jacobsen, S.B., Knoll, A.H., 1993. The Vendian record of Sr and C isotopic variations in seawater: Implications for tectonics and paleoclimate. Earth Planet. Sci. Lett. https://doi.org/10.1016/0012-821X(93)90254-7

Kaufman, A.J., Knoll, A.H., 1995. Neoproterozoic variations in the C-isotopic composition of seawater: stratigraphic and biogeochemical implications. Precambrian Res. https://doi.org/10.1016/0301-9268(94)00070-8

Keller, C.B., Harrison, T.M., 2020. Constraining crustal silica on ancient Earth. Proc. Natl. Acad. Sci. U. S. A. 117. https://doi.org/10.1073/pnas.2009431117

Knoll, A.H., 2014. Paleobiological perspectives on early eukaryotic evolution. Cold Spring Harb. Perspect. Biol. 6. https://doi.org/10.1101/cshperspect.a016121

Knoll, A.H., 1994. Proterozoic and early Cambrian protists: Evidence for accelerating evolutionary tempo. Proc. Natl. Acad. Sci. U. S. A. 91. https://doi.org/10.1073/pnas.91.15.6743

Knoll, A.H., Golubic, S., 1992. Proterozoic and Living Cyanobacteria, in: Early Organic Evolution. https://doi.org/10.1007/978-3-642-76884-2_35

Knoll, A.H., Hayes, J.M., Kaufman, A.J., Swett, K., Lambert, I.B., 1986. Secular variation in carbon isotope ratios from Upper Proterozoic successions of Svalbard and East Greenland. Nature 321. https://doi.org/10.1038/321832a0

Knoll, A.H., Javaux, E.J., Hewitt, D., Cohen, P., 2006. Eukaryotic organisms in Proterozoic oceans. Philos. Trans. R. Soc. B Biol. Sci. 361, 1023–1038. https://doi.org/10.1098/rstb.2006.1843

Knoll, A.H., Kaufman, A.J., Semikhatov, M.A., 1995. The carbon-isotopic composition of Proterozoic carbonates: Riphean successions from northwestern Siberia (Anabar Massif, Turukhansk uplift). Am. J. Sci. 295. https://doi.org/10.2475/ajs.295.7.823

Knoll, A.H., Nowak, M.A., 2017. The timetable of evolution. Sci. Adv. 3, 1–14. https://doi.org/10.1126/sciadv.1603076

Kochnev, B.B., Pokrovsky, B.G., Kuznetsov, A.B., Marusin, V. V., 2018. C and Sr isotope chemostratigraphy of Vendian-Lower Cambrian carbonate sequences in the central Siberian Platform. Russ. Geol. Geophys. 59, 585–605. https://doi.org/10.1016/j.rgg.2018.05.001

Komiya, T., Maruyama, S., Masuda, T., Nohda, S., Hayashi, M., Okamoto, K., 1999. Plate tectonics at 3.8-3.7 Ga: Field evidence from the Isua Accretionary Complex, southern West Greenland. J. Geol. 107. https://doi.org/10.1086/314371

Kopp, R.E., Kirschvink, J.L., Hilburn, I.A., Nash, C.Z., 2005. The paleoproterozoic

snowball Earth: A climate disaster triggered by the evolution of oxygenic photosynthesis. Proc. Natl. Acad. Sci. U. S. A. 102, 11131–11136. https://doi.org/10.1073/pnas.0504878102

Koppes, M.N., Montgomery, D.R., 2009. The relative efficacy of fluvial and glacial erosion over modern to orogenic timescales. Nat. Geosci. 2. https://doi.org/10.1038/ngeo616

Kröner, A., Layer, P.W., 1992. Crust formation and plate motion in the early Archean. Science (80-.). https://doi.org/10.1126/science.256.5062.1405

Kupecz, J.A., Land, L.S., 1991. Late-stage dolomitization of the Lower Ordovician Ellenburger Group, west Texas. J. Sediment. Petrol. https://doi.org/10.1306/D426775D-2B26-11D7-8648000102C1865D

Kuznetsov, A.B., Bekker, A., Ovchinnikova, G. V., Gorokhov, I.M., Vasilyeva, I.M., 2017. Unradiogenic strontium and moderate-amplitude carbon isotope variations in early Tonian seawater after the assembly of Rodinia and before the Bitter Springs Excursion. Precambrian Res. 298, 157–173. https://doi.org/10.1016/j.precamres.2017.06.011

Kuznetsov, A.B., Gorokhov, I.M., Azimov, P.Y., Dubinina, E.O., 2021. Sr- and C-Chemostratigraphy Potential of the Paleoproterozoic Sedimentary Carbonates under Medium-Temperature Metamorphism: the Ruskeala Marble, Karelia. Petrology 29. https://doi.org/10.1134/S0869591121010033

Kuznetsov, A.B., Gorokhov, I.M., Melezhik, V.A., Mel'nikov, N.N., Konstantinova, G. V., Turchenko, T.L., 2012. Strontium isotope composition of the lower proterozoic carbonate concretions: The Zaonega Formation, Southeast Karelia.

Lithol. Miner. Resour. 47, 319–333. https://doi.org/10.1134/S0024490212030066

Kuznetsov, A.B., Kochnev, B.B., Vasilyeva, I.M., Ovchinnikova, G. V., 2019a. The Upper Riphean of the Yenisei Range: Sr Chemostratigraphy and Pb–Pb Age of Limestones of the Tungusik and Shirokaya Groups. Stratigr. Geol. Correl. 27. https://doi.org/10.1134/S0869593819050058

Kuznetsov, A.B., Krupenin, M.T., Ovchinnikova, G. V., Gorokhov, I.M., Maslov, A. V., Kaurova, O.K., Ellmies, R., 2005. Diagenesis of carbonate and siderite deposits of the Lower Riphean Bakal Formation, the southern Urals: Sr isotopic characteristics and Pb-Pb age. Lithol. Miner. Resour. 40, 195–215. https://doi.org/10.1007/s10987-005-0022-z

Kuznetsov, A.B., Lobach–Zhuchenko, S.B., Kaulina, T. V., Konstantinova, G. V., 2019b. Paleoproterozoic Age of Carbonates and Trondhjemites of the Central Azov Group: Sr Isotope Chemostratigraphy and U–Pb Geochronology. Dokl. Earth Sci. 484. https://doi.org/10.1134/S1028334X19020211

Kuznetsov, A.B., Melezhik, V.A., Gorokhov, I.M., Mel'nikov, N.N., Fallick, A.E., 2003a. Sr isotope composition in paleoproterozoic carbonates extremely enriched in13C: Kaniapiskau supergroup, the Labrador trough of the Canadian Shield. Stratigr. Geol. Correl. 11, 209–219.

Kuznetsov, A.B., Melezhik, V.A., Gorokhov, I.M., Melnikov, N.N., Konstantinova, G. V., Kutyavin, E.P., Turchenko, T.L., 2010. Sr isotopic composition of Paleoproterozoic 13C-rich carbonate rocks: The Tulomozero Formation, SE Fennoscandian Shield. Precambrian Res. 182, 300–312. https://doi.org/10.1016/j.precamres.2010.05.006

Kuznetsov, A.B., Ovchinnikova, G. V., Semikhatov, M.A., Gorokhov, I.M., Kaurova, O.K., Krupenin, M.T., Vasil'eva, I.M., Gorokhovskii, B.M., Maslov, A. V., 2008. The Sr isotopic characterization and Pb-Pb age of carbonate rocks from the Satka formation, the Lower Riphean Burzyan Group of the southern Urals. Stratigr. Geol. Correl. 16, 120–137. https://doi.org/10.1134/S0869593808020020

Kuznetsov, A.B., Semikhatov, M.A., Gorokhov, I.M., 2018. Strontium isotope stratigraphy: principles and state-of-the-art. Stratigr. Geol. Correl. 26, 367-386. 10.1134/S0869593818040056

Kuznetsov, A.B., Semikhatov, M.A., Gorokhov, I.M., Mel'nikov, N.N., Konstantinova, G. V., Kutyavin, E.P., 2003b. Sr isotope composition in carbonates of the Karatau Group, southern Urals, and standard curve of 87Sr/86Sr variations in the Late Riphean Ocean. Stratigr. Geol. Correl. 11, 415–449.

Kuznetsov, A.B., Semikhatov, M.A., Maslov, A. V., Gorokhov, I.M., Prasolov, E.M., Krupenin, M.T., Kislova, I. V., 2006. New data on Sr-and C-isotopic chemostratigraphy of the Upper Riphean type section (southern Urals). Stratigr. Geol. Correl. 14, 602–628. https://doi.org/10.1134/S0869593806060025

Lamb, D.M., Awramik, S.M., Chapman, D.J., Zhu, S., 2009. Evidence for eukaryotic diversification in the ~1800 million-year-old Changzhougou Formation, North China. Precambrian Res. 173. https://doi.org/10.1016/j.precamres.2009.05.005

Lenton, T.M, Crouch, M., Johnson, M., Pires, N., Dolan, L., 2012. First plants cooled the Ordovician. Nature Geoscience 86–89. https://doi.org/10.1038/ngeo1390.

Lenton, T.M., Watson, A.J., 2004. Biotic enhancement of weathering, atmospheric oxygen and carbon dioxide in the Neoproterozoic. Geophys. Res. Lett. 31, n/a-n/a.

https://doi.org/10.1029/2003gl018802

Li, D., Shields-Zhou, G.A., Ling, H.F., Thirlwall, M., 2011. Dissolution methods for strontium isotope stratigraphy: Guidelines for the use of bulk carbonate and phosphorite rocks. Chem. Geol. https://doi.org/10.1016/j.chemgeo.2011.09.004

Li, Y., Li, C., Guo, J., 2020. Re-evaluation and optimisation of dissolution methods for strontium isotope stratigraphy based on chemical leaching of carbonate certificated reference materials. Microchem. J. 154. https://doi.org/10.1016/j.microc.2020.104607

Lipp, A.G., Shorttle, O., Sperling, E.A., Brocks, J.J., Cole, D.B., Crockford, P.W., Del Mouro, L., Dewing, K., Dornbos, S.Q., Emmings, J.F., Farrell, U.C., Jarrett, A., Johnson, B.W., Kabanov, P., Keller, C.B., Kunzmann, M., Miller, A.J., Mills, N.T., O'Connell, B., Peters, S.E., Planavsky, N.J., Ritzer, S.R., Schoepfer, S.D., Wilby, P.R., Yang, J., 2021. The composition and weathering of the continents over geologic time. Geochemical Perspect. Lett. 17. https://doi.org/10.7185/geochemlet.2109

Liu, C., Wang, Z., Raub, T.D., 2013. Geochemical constraints on the origin of Marinoan cap dolostones from Nuccaleena Formation, South Australia. Chem. Geol. 351, 95–104. https://doi.org/10.1016/j.chemgeo.2013.05.012

Liu, C., Wang, Z., Raub, T.D., Macdonald, F.A., Evans, D.A.D., 2014. Neoproterozoic cap-dolostone deposition in stratified glacial meltwater plume. Earth Planet. Sci. Lett. 404, 22–32. https://doi.org/10.1016/j.epsl.2014.06.039

Liu, X.M., Kah, L.C., Knoll, A.H., Cui, H., Wang, C., Bekker, A., Hazen, R.M., 2021. A persistently low level of atmospheric oxygen in Earth's middle age. Nat.

Commun. 12, 1–7. https://doi.org/10.1038/s41467-020-20484-7

Macdonald, F.A., Strauss, J. V., Sperling, E.A., Halverson, G.P., Narbonne, G.M., Johnston, D.T., Kunzmann, M., Schrag, D.P., Higgins, J.A., 2013. The stratigraphic relationship between the Shuram carbon isotope excursion, the oxygenation of Neoproterozoic oceans, and the first appearance of the Ediacara biota and bilaterian trace fossils in northwestern Canada. Chem. Geol. 362, 250–272. https://doi.org/10.1016/j.chemgeo.2013.05.032

Marshall, J.D., 1992. Climatic and oceanographic isotopic signals from the carbonate rock record and their preservation. Geol. Mag. https://doi.org/10.1017/S0016756800008244

Martin, A.P., Condon, D.J., Prave, A.R., Lepland, A., 2013. Earth-Science Reviews A review of temporal constraints for the Palaeoproterozoic large , positive carbonate carbon isotope excursion (the Lomagundi – Jatuli Event). Earth Sci. Rev. 127, 242–261. https://doi.org/10.1016/j.earscirev.2013.10.006

Mazzullo, S.J., 1992. Geochemical and neomorphic alteration of dolomite: A review. Carbonates and Evaporites. https://doi.org/10.1007/BF03175390

McArthur, J., Howarth, R.J., 2005. Strontium isotope stratigraphy, in: A Geologic Time Scale 2004. https://doi.org/10.1017/CBO9780511536045.008

McArthur, J.M., 1994. Recent trends in strontium isotope stratigraphy. Terra Nov. https://doi.org/10.1111/j.1365-3121.1994.tb00507.x

McArthur, J.M., Howarth, R.J., Bailey, T.R., 2001. Strontium isotope stratigraphy: LOWESS version 3: Best fit to the marine Sr-isotope curve for 0-509 Ma and

accompanying look-up table for deriving numerical age. J. Geol. https://doi.org/10.1086/319243

McArthur, J.M., Howarth, R.J., Shields, G.A., 2012. Strontium Isotope Stratigraphy. Geol. Time Scale 2012 1–2, 127–144. https://doi.org/10.1016/B978-0-444-59425-9.00007-X

McCulloch, M.T., 1994. Primitive 87Sr86Sr from an Archean barite and conjecture on the Earth's age and origin. Earth Planet. Sci. Lett. 126, 1–13. https://doi.org/10.1016/0012-821X(94)90238-0

Melezhik, V.A., Fallick, A.E., Rychanchik, D. V., Kuznetsov, A.B., 2005. Palaeoproterozoic evaporites in Fennoscandia: Implications for seawater sulphate, the rise of atmospheric oxygen and local amplification of the δ13C excursion. Terra Nov. 17, 141–148. https://doi.org/10.1111/j.1365-3121.2005.00600.x

Melezhik, V.A., Pokrovsky, B.G., Fallick, A.E., Kuznetsov, A.B., Bujakaite, M.I., 2009. Constraints on 87Sr/86Sr of late Ediacaran seawater: Insight from Siberian high-Sr limestones. J. Geol. Soc. London. 166, 183–191. https://doi.org/10.1144/0016-76492007-171

Melim, L.A., Swart, P.K., Eberli, G.P., 2004. Mixing-Zone Diagenesis in the Subsurface of Florida and the Bahamas. J. Sediment. Res. https://doi.org/10.1306/042904740904

Merdith, A.S., Collins, A.S., Williams, S.E., Pisarevsky, S., Foden, J.D., Archibald, D.B., Blades, M.L., Alessio, B.L., Armistead, S., Plavsa, D., Clark, C., Müller, R.D., 2017. A full-plate global reconstruction of the Neoproterozoic. Gondwana Res. 50, 84–134. https://doi.org/10.1016/j.gr.2017.04.001

Miao, L., Moczydłowska, M., Zhu, S., Zhu, M., 2019. New record of organic-walled, morphologically distinct microfossils from the late Paleoproterozoic Changcheng Group in the Yanshan Range, North China. Precambrian Res. 321, 172–198. https://doi.org/10.1016/j.precamres.2018.11.019

Miller, N., Johnson, P.R., Stern, R.J., 2008. Marine versus non-marine environments for the Jibalah Group, NW Arabian shield: A sedimentologic and geochemical survey and report of possible metazoa in the Dhaiqa formation. Arab. J. Sci. Eng.

Miller, N.R., Stern, R.J., Avigad, D., Beyth, M., Schilman, B., 2009. Cryogenian slate-carbonate sequences of the Tambien Group, Northern Ethiopia (I): Pre-"Sturtian" chemostratigraphy and regional correlations. Precambrian Res. 170, 129–156. https://doi.org/10.1016/j.precamres.2008.12.004

Millet, M.A., Dauphas, N., Greber, N.D., Burton, K.W., Dale, C.W., Debret, B., Macpherson, C.G., Nowell, G.M., Williams, H.M., 2016. Titanium stable isotope investigation of magmatic processes on the Earth and Moon. Earth Planet. Sci. Lett. 449. https://doi.org/10.1016/j.epsl.2016.05.039

Montañez, I.P., Banner, J.L., Osleger, D.A., Borg, L.E., Bosserman, P.J., 1996. Integrated Sr isotope variations and sea-level history of middle to Upper Cambrian platform carbonates: Implications for the evolution of Cambrian seawater 87Sr/86Sr. Geology. https://doi.org/10.1130/0091-7613(1996)024<0917:ISIVAS>2.3.CO;2

Morse, J.W., Mackenzie, F.T., 1990. Geochemistry of sedimentary carbonates. Geochemistry Sediment. carbonates. https://doi.org/10.1016/0016-7037(93)90401-h

1649 Moyen, J.F., Stevens, G., Kisters, A., 2006. Record of mid-Archaean subduction from
1650 metamorphism in the Barberton terrain, South Africa. Nature 442.
1651 https://doi.org/10.1038/nature04972

1652 Nogueira, A.C.R., Riccomini, C., Sial, A.N., Moura, C.A.V., Trindade, R.I.F., Fairchild,
1653 T.R., 2007. Carbon and strontium isotope fluctuations and paleoceanographic
1654 changes in the late Neoproterozoic Araras carbonate platform, southern Amazon
1655 craton, Brazil. Chem. Geol. 237, 168–190.
1656 https://doi.org/10.1016/j.chemgeo.2006.06.016

1657 Northrop, D.A., Clayton, R.N., 1966. Oxygen-Isotope Fractionations in Systems
1658 Containing Dolomite. J. Geol. https://doi.org/10.1086/627153

1659 Nutman, A.P., Friend, C.R.L., Bennett, V.C., 2002. Evidence for 3650-3600 Ma
1660 assembly of the northern end of the Itsaq Gneiss Complex, Greenland: Implication
1661 for early Archaean tectonics. Tectonics 21. https://doi.org/10.1029/2000tc001203

1662 Och, L.M., Shields-Zhou, G.A., 2012. The Neoproterozoic oxygenation event:
1663 Environmental perturbations and biogeochemical cycling. Earth-Science Rev. 110,
1664 26–57. https://doi.org/10.1016/j.earscirev.2011.09.004

1665 Oelkers, E.H., Jones, M.T., Pearce, C.R., Jeandel, C., Eiriksdottir, E.S., Gislason, S.R.,
1666 2012. Riverine particulate material dissolution in seawater and its implications for
1667 the global cycles of the elements. Comptes Rendus - Geosci.
1668 https://doi.org/10.1016/j.crte.2012.08.005

1669 Ovchinnikova, G., Gorokhov, I., Belyatskii, B., 1995. U-Pb systematics of pre-
1670 Cambrian carbonates: The Riphean Sukhaya Tunguska Formation in the
1671 Turukhansk Uplift, Siberia. Lithol. Miner. Resour. 30.

1672 Paytan, A., Kastner, M., Martin, E.E., MacDougall, J.D., Herbert, T., 1993. Marine
1673 barite as a monitor of seawater strontium isotope composition. Nature 366, 445–
1674 449. https://doi.org/10.1038/366445a0

1675 Piper, J.D.A., 2010. Protopangaea: Palaeomagnetic definition of Earth's oldest (mid-
1676 Archaean-Palaeoproterozoic) supercontinent. J. Geodyn.
1677 https://doi.org/10.1016/j.jog.2010.01.002

1678 Pokrovskiy, B.G., Vinogradov, V.I., 1994. Isotopic composition of strontium, oxygen
1679 and carbon in upper precambrian carbonates of the western slope of the Anabar
1680 rise (Kotyykan river area). Dokl. Earth Sci. Sect.

1681 Pollock, M.D., Kah, L.C., Bartley, J.K., 2006. Morphology of molar-tooth structures in
1682 Precambrian carbonates: Influence of substrate rheology and implications for
1683 genesis. J. Sediment. Res. 76. https://doi.org/10.2110/jsr.2006.021

1684 Poulton, S.W., Bekker, A., Cumming, V.M., Zerkle, A.L., Canfield, D.E., Johnston,
1685 D.T., 2021. A 200-million-year delay in permanent atmospheric oxygenation.
1686 Nature 592. https://doi.org/10.1038/s41586-021-03393-7

1687 Prokoph, A., El Bilali, H., Ernst, R., 2013. Periodicities in the emplacement of large
1688 igneous provinces through the Phanerozoic: Relations to ocean chemistry and
1689 marine biodiversity evolution. Geosci. Front. 4.
1690 https://doi.org/10.1016/j.gsf.2012.08.001

1691 Prokoph, A., Shields, G.A., Veizer, J., 2008. Compilation and time-series analysis of a
1692 marine carbonate δ18O, δ13C, 87Sr/86Sr and δ34S database through Earth history.
1693 Earth-Science Rev. 87, 113–133. https://doi.org/10.1016/j.earscirev.2007.12.003

1694 Ravindran, A., Mezger, K., Balakrishnan, S., Kooijman, E., Schmitt, M., Berndt, J.,
1695 2020. Initial 87Sr/86Sr as a sensitive tracer of Archaean crust-mantle evolution:
1696 Constraints from igneous and sedimentary rocks in the western Dharwar Craton,
1697 India. Precambrian Res. 337, 105523.
1698 https://doi.org/10.1016/j.precamres.2019.105523

1699 Ray, J.S., Veizer, J., Davis, W.J., 2003. C, O, Sr and Pb isotope systematics of carbonate
1700 sequences of the Vindhyan Supergroup, India: Age, diagenesis, correlations and
1701 implications for global events. Precambrian Res. 121, 103–140.
1702 https://doi.org/10.1016/S0301-9268(02)00223-1

1703 Raymo, M.E., Ruddiman, W.F., Froelich, P.N., 1988. Influence of late Cenozoic
1704 mountain building on ocean geochemical cycles. Geology.
1705 https://doi.org/10.1130/0091-7613(1988)016<0649:IOLCMB>2.3.CO;2

1706 Rimstidt, J.D., Balog, A., Webb, J., 1998. Distribution of trace elements between
1707 carbonate minerals and aqueous solutions. Geochim. Cosmochim. Acta 62.
1708 https://doi.org/10.1016/S0016-7037(98)00125-2

1709 Rino, S., Komiya, T., Windley, B.F., Katayama, I., Motoki, A., Hirata, T., 2004. Major
1710 episodic increases of continental crustal growth determined from zircon ages of
1711 river sands; implications for mantle overturns in the Early Precambrian. Phys.
1712 Earth Planet. Inter. 146. https://doi.org/10.1016/j.pepi.2003.09.024

1713 Rogers, J.J.W., Santosh, M., 2002. Configuration of Columbia, a Mesoproterozoic
1714 Supercontinent. Gondwana Res. 5. https://doi.org/10.1016/S1342-
1715 937X(05)70883-2

1716 Rooney, A.D., Macdonald, F.A., Strauss, J. V., Dudás, F.Ö., Hallmann, C., Selby, D.,

2014. Re-Os geochronology and coupled Os-Sr isotope constraints on the Sturtian snowball Earth. Proc. Natl. Acad. Sci. U. S. A. 111, 51–56. https://doi.org/10.1073/pnas.1317266110

Rothman, D.H., Hayes, J.M., Summons, R.E., 2003. Dynamics of the Neoproterozoic carbon cycle. Proc. Natl. Acad. Sci. U. S. A. https://doi.org/10.1073/pnas.0832439100

Rubinson, M., Clayton, R.N., 1969. Carbon-13 fractionation between aragonite and calcite. Geochim. Cosmochim. Acta. https://doi.org/10.1016/0016-7037(69)90109-4

Ruddiman, W.F., Raymo, M.E., Prell, W.L., Kutzbach, J.E., 1997. The Uplift-Climate Connection: A Synthesis, in: Tectonic Uplift and Climate Change. https://doi.org/10.1007/978-1-4615-5935-1_20

Rye, R., Holland, H.D., 1998. Paleosols and the evolution of atmospheric oxygen: A critical review. Am. J. Sci. 298. https://doi.org/10.2475/ajs.298.8.621

Saltzman, M.R., 2005. Phosphorus, nitrogen, and the redox evolution of the Paleozoic oceans. Geology. https://doi.org/10.1130/G21535.1

Satkoski, A.M., Fralick, P., Beard, B.L., Johnson, C.M., 2017. Initiation of modern-style plate tectonics recorded in Mesoarchean marine chemical sediments. Geochim. Cosmochim. Acta 209, 216–232. https://doi.org/10.1016/j.gca.2017.04.024

Satkoski, A.M., Lowe, D.R., Beard, B.L., Coleman, M.L., Johnson, C.M., 2016. A high continental weathering flux into Paleoarchean seawater revealed by strontium

isotope analysis of 3.26 Ga barite. Earth Planet. Sci. Lett. 454, 28–35. https://doi.org/10.1016/j.epsl.2016.08.032

Satkoski, A.M., Lowe, D.R., Beard, B.L., Coleman, M.L., Johnson, C.M., Street, W.D., States, U., States, U., Africa, S., n.d. Supplementary Material for : A high continental weathering flux into Paleoarchean seawater revealed by strontium isotope analysis of 3 . 26 Ga barite NASA Astrobiology Institute , United States Stanford University , Department of Geological and Environmen 00002, 987.

Sawaki, Y., Kawai, T., Shibuya, T., Tahata, M., Omori, S., Komiya, T., Yoshida, N., Hirata, T., Ohno, T., Windley, B.F., Maruyama, S., 2010a. 87Sr/86Sr chemostratigraphy of Neoproterozoic Dalradian carbonates below the Port Askaig Glaciogenic Formation, Scotland. Precambrian Res. 179, 150–164. https://doi.org/10.1016/j.precamres.2010.02.021

Sawaki, Y., Ohno, T., Tahata, M., Komiya, T., Hirata, T., Maruyama, S., Windley, B.F., Han, J., Shu, D., Li, Y., 2010b. The Ediacaran radiogenic Sr isotope excursion in the Doushantuo Formation in the Three Gorges area, South China. Precambrian Res. 176, 46–64. https://doi.org/10.1016/j.precamres.2009.10.006

Schidlowski, M., Eichmann, R., Junge, C.E., 1975. Precambrian sedimentary carbonates: carbon and oxygen isotope geochemistry and implications for the terrestrial oxygen budget. Precambrian Res. 2. https://doi.org/10.1016/0301-9268(75)90018-2

Schrag, D.P., Higgins, J.A., Macdonald, F.A., Johnston, D.T., 2013. Authigenic carbonate and the history of the global carbon cycle. Science (80-.). 339. https://doi.org/10.1126/science.1229578

Semikhatov, M.A., 2002. Low 87 Sr / 86 Sr Ratios in Seawater of the Grenville and post-Grenville Time : Determining Factors.

Semikhatov, M.A., Ovchinnikova, G. V., Gorokhov, I.M., Kuznetsov, A.B., Kaurova, O.K., Petrov, P.Y., 2004. Pb-Pb isochronous age and Sr-isotopic signature of the Upper Yudoma carbonate sediments (the Vendian of the Yudoma-Maya trough, Eastern Siberia). Dokl. Akad. Nauk 393, 83–87.

Shi, M., Shi, M., Feng, Q., Zareen, M., Zhu, S., 2017. An Eukaryote-Bearing Microbiota From The Early Mesoproterozoic Gaoyuzhuang Formation , Tianjin , China And Its Significance An eukaryote-bearing microbiota from the early mesoproterozoic Gaoyuzhuang Formation , Tianjin , China and its signi fi cance. Precambrian Res. 0–1. https://doi.org/10.1016/j.precamres.2017.09.013

Shields-Zhou, G., Och, L., 2011. The case for a neoproterozoic oxygenation event: Geochemical evidence and biological consequences. GSA Today 21, 4–11. https://doi.org/10.1130/GSATG102A.1

Shields, G., Stille, P., Brasier, M.D., Atudorei, N.V., 1997. Stratified oceans and oxygenation of the late Precambrian environment: a post glacial geochemical record from the Neoproterozoic of W Mongolia. Terra Nov. 9. https://doi.org/10.1111/j.1365-3121.1997.tb00016.x

Shields, G., Veizer, J., 2002. Precambrian marine carbonate isotope database: Version 1.1. Geochemistry, Geophys. Geosystems 3. https://doi.org/10.1029/2001GC000266

Shields, G. A., 2007. A normalised seawater strontium isotope curve: possible implications for Neoproterozoic-Cambrian weathering rates and the further

oxygenation of the Earth. eEarth. https://doi.org/10.5194/ee-2-35-2007

Shields, G.A., 2002. “Molar-tooth microspar”: A chemical explanation for its disappearance ~ 750 Ma. Terra Nov. https://doi.org/10.1046/j.1365-3121.2002.00396.x

Shields, G.A., Carden, G.A.F., Veizer, J., Meidla, T., Rong, J.Y., Li, R.Y., 2003. Sr, C, and O isotope geochemistry of Ordovician brachiopods: A major isotopic event around the Middle-Late Ordovician transition. Geochim. Cosmochim. Acta 67. https://doi.org/10.1016/S0016-7037(02)01116-X

Shields, G.A., Mills, B.J.W., Zhu, M., Raub, T.D., Daines, S.J., Lenton, T.M., 2019. Unique Neoproterozoic carbon isotope excursions sustained by coupled evaporite dissolution and pyrite burial. Nat. Geosci. 12, 823–827. https://doi.org/10.1038/s41561-019-0434-3

Smith, A.G., 1968. The Origin and Deformation of Some “Molar-Tooth” Structures in the Precambrian Belt-Purcell Supergroup. J. Geol. 76. https://doi.org/10.1086/627341

Smithies, R.H., Van Kranendonk, M.J., Champion, D.C., 2007. The Mesoarchean emergence of modern-style subduction. Gondwana Res. 11. https://doi.org/10.1016/j.gr.2006.02.001

Spencer, C.J., Cawood, P.A., Hawkesworth, C.J., Raub, T.D., Prave, A.R., Roberts, N.M.W., 2014. Proterozoic onset of crustal reworking and collisional tectonics: Reappraisal of the zircon oxygen isotope record. Geology. https://doi.org/10.1130/G35363.1

1807 Spencer, C.J., Hawkesworth, C., Cawood, P.A., Dhuime, B., 2013. Not all
1808 supercontinents are created equal: Gondwana-rodinia case study. Geology 41,
1809 795–798. https://doi.org/10.1130/G34520.1

1810 Spooner, E.T.C., 1976. The strontium isotopic composition of seawater, and seawater-
1811 oceanic crust interaction. Earth Planet. Sci. Lett. https://doi.org/10.1016/0012-
1812 821X(76)90108-4

1813 Steiger, R.H., Jäger, E., 1977. Subcommission on geochronology: Convention on the
1814 use of decay constants in geo- and cosmochronology. Earth Planet. Sci. Lett. 36.
1815 https://doi.org/10.1016/0012-821X(77)90060-7

1816 Stern, R.J., 2018. The evolution of plate tectonics. Philos. Trans. R. Soc. A Math. Phys.
1817 Eng. Sci. 376. https://doi.org/10.1098/rsta.2017.0406

1818 Stüeken, E.E., Bellefroid, E.J., Prave, A., Asael, D., Planavsky, N.J., Lyons, T.W., 2017.
1819 Not so non-marine? Revisiting the Stoer Group and the Mesoproterozoic
1820 biosphere. Geochemical Perspect. Lett. https://doi.org/10.7185/geochemlet.1725

1821 Sun, X., Turchyn, A. V., 2014. Significant contribution of authigenic carbonate to
1822 marine carbon burial. Nat. Geosci. 7. https://doi.org/10.1038/ngeo2070

1823 Swart, P.K., 2015. The geochemistry of carbonate diagenesis: The past, present and
1824 future. Sedimentology. https://doi.org/10.1111/sed.12205

1825 Tang, D., Shi, X., Wang, X., Jiang, G., 2016. Extremely low oxygen concentration in
1826 mid-Proterozoic shallow seawaters. Precambrian Res. 276, 145–157.
1827 https://doi.org/10.1016/j.precamres.2016.02.005

1828 Tang, M., Chen, K., Rudnick, R.L., 2016. Archean upper crust transition from mafic to

felsic marks the onset of plate tectonics. Science (80-.). 351. https://doi.org/10.1126/science.aad5513

Tang, Q., Pang, K., Yuan, X., Xiao, S., 2020. A one-billion-year-old multicellular chlorophyte. Nat. Ecol. Evol. https://doi.org/10.1038/s41559-020-1122-9

Taylor, S.R., McLennan, S.M., 1985. The Continental Crust: its Composition and Evolution. An Examination of the Geochemical Record Preserved in Sedimentary Rocks., The Continental Crust: its Composition and Evolution. An Examination of the Geochemical Record Preserved in Sedimentary Rocks.

Thomas, C.W., Graham, C.M., Ellam, R.M., Fallick, A.E., 2004. 87Sr/86SR chemostratigraphy of Neoproterozoic Dalradian limestones Scotland and Ireland: Constraints on depositional ages and time scales. J. Geol. Soc. London. 161, 229–242. https://doi.org/10.1144/0016-764903-001

Torres, M.A., Moosdorf, N., Hartmann, J., Adkins, J.F., West, A.J., 2017. Glacial weathering, sulfide oxidation, and global carbon cycle feedbacks. Proc. Natl. Acad. Sci. U. S. A. 114, 8716–8721. https://doi.org/10.1073/pnas.1702953114

Torres, M.A., West, A.J., Li, G., 2014. Sulphide oxidation and carbonate dissolution as a source of CO2 over geological timescales. Nature 507, 346–349. https://doi.org/10.1038/nature13030

Torres, M.E., Hong, W.L., Solomon, E.A., Milliken, K., Kim, J.H., Sample, J.C., Teichert, B.M.A., Wallmann, K., 2020. Silicate weathering in anoxic marine sediment as a requirement for authigenic carbonate burial. Earth-Science Rev. https://doi.org/10.1016/j.earscirev.2019.102960

Tyrrell, T., 1999. The relative influences of nitrogen and phosphorus on oceanic primary production. Nature. https://doi.org/10.1038/22941

Vahrenkamp, V.C., Swart, P.K., 1990. New distribution coefficient for the incorporation of strontium into dolomite and its implications for the formation of ancient dolomites. Geology 18. https://doi.org/10.1130/0091-7613(1990)018<0387:NDCFTI>2.3.CO;2

Valladares, M.I., Ugidos, J.M., Barba, P., Fallick, A.E., Ellam, R.M., 2006. Oxygen, carbon and strontium isotope records of Ediacaran carbonates in Central Iberia (Spain). Precambrian Res. 147, 354–365. https://doi.org/10.1016/j.precamres.2006.01.021

Valley, J.W., 2003. Oxygen isotopes in zircon. Rev. Mineral. Geochemistry 53. https://doi.org/10.2113/0530343

Van Geldern, R., Joachimski, M.M., Day, J., Jansen, U., Alvarez, F., Yolkin, E.A., Ma, X.P., 2006. Carbon, oxygen and strontium isotope records of Devonian brachiopod shell calcite. Palaeogeogr. Palaeoclimatol. Palaeoecol. https://doi.org/10.1016/j.palaeo.2006.03.045

Van Kranendonk, M.J., 2010. Two types of Archean continental crust: Plume and plate tectonics on early earth. Am. J. Sci. 310. https://doi.org/10.2475/10.2010.01

Van Kranendonk, M.J., Hugh Smithies, R., Hickman, A.H., Champion, D.C., 2007. Review: Secular tectonic evolution of Archean continental crust: interplay between horizontal and vertical processes in the formation of the Pilbara Craton, Australia. Terra Nov. 19, 1–38. https://doi.org/10.1111/j.1365-3121.2006.00723.x

1873 Vasconcelos, C., McKenzie, J.A., Warthmann, R., Bernasconi, S.M., 2005. Calibration
1874 of the δ18O paleothermometer for dolomite precipitated in microbial cultures and
1875 natural environments. Geology. https://doi.org/10.1130/G20992.1

1876 Veizer, J., 1989. Strontium Isotopes in Seawater Through Time Strontium Isotope
1877 Systematics. Ann. Rev. Earth Planet. Sci 17, 14167.

1878 Veizer, J., 1983. Chemical diagenesis of carbonates: theory and application of trace
1879 element technique. Stable Isot. Sediment. Geol.

1880 Veizer, J., Ala, D., Azmy, K., Bruckschen, P., Buhl, D., Bruhn, F., Garden, G.A.F.,
1881 Diener, A., Ebneth, S., Godderis, Y., Jasper, T., Korte, C., Pawellek, F., Podlaha,
1882 O.G., Strauss, H., 1999. 87Sr/86Sr, δ13C and δ18O evolution of Phanerozoic
1883 seawater. Chem. Geol. https://doi.org/10.1016/S0009-2541(99)00081-9

1884 Veizer, J., Buhl, D., Diener, A., Ebneth, S., Podlaha, O.G., Bruckschen, P., Jasper, T.,
1885 Korte, C., Schaaf, M., Ala, D., Azmy, K., 1997. Strontium isotope stratigraphy:
1886 Potential resolution and event correlation. Palaeogeogr. Palaeoclimatol.
1887 Palaeoecol. https://doi.org/10.1016/S0031-0182(97)00054-0

1888 Veizer, J., Clayton, R.N., Hinton, R.W., 1992a. Geochemistry of precambrian
1889 carbonates: IV. Early paleoproterozoic (2.25 ± 0.25 ga) seawater. Geochim.
1890 Cosmochim. Acta 56, 875–885. https://doi.org/10.1016/0016-7037(92)90033-F

1891 Veizer, J., Compston, W., 1976. 87Sr/86Sr in Precambrian carbonates as an index of
1892 crustal evolution. Geochim. Cosmochim. Acta 40, 905–914.
1893 https://doi.org/10.1016/0016-7037(76)90139-3

1894 Veizer, J., Compston, W., 1974. 87Sr/86Sr composition of seawater during the

Phanerozoic. Geochim. Cosmochim. Acta. https://doi.org/10.1016/0016-7037(74)90099-4

Veizer, J., Hoefs, J., Lowe, D.R., Thurston, P.C., 1989. Geochemistry of Precambrian carbonates: II. Archean greenstone belts and Archean sea water. Geochim. Cosmochim. Acta 53. https://doi.org/10.1016/0016-7037(89)90031-8

Veizer, J., Plumb, K.A., Clayton, R.N., Hinton, R.W., Grotzinger, J.P., 1992b. Geochemistry of Precambrian carbonates: V. Late Paleoproterozoic seawater. Geochim. Cosmochim. Acta 56, 2487–2501. https://doi.org/10.1016/0016-7037(92)90204-V

Voice, P.J., Kowalewski, M., Eriksson, K.A., 2011. Quantifying the timing and rate of crustal evolution: Global compilation of radiometrically dated detrital zircon grains. J. Geol. 119, 109–126. https://doi.org/10.1086/658295

Walker, D.A., Sivak, M.N., Prinsley, R.T., Cheesbrough, J.K., 1983. Simultaneous Measurement of Oscillations in Oxygen Evolution and Chlorophyll a Fluorescence in Leaf Pieces . Plant Physiol. 73. https://doi.org/10.1104/pp.73.3.542

Walker, J.C.G., Hays, P.B., Kasting, J.F., 1981. A negative feedback mechanism for the long-term stabilization of Earth's surface temperature. J. Geophys. Res. https://doi.org/10.1029/JC086iC10p09776

Wang, C., Mitchell, R.N., Murphy, J.B., Peng, P., Spencer, C.J., 2021. The role of megacontinents in the supercontinent cycle. Geology 49. https://doi.org/10.1130/G47988.1

Wanke, A., Melezhik, V., 2005. Sedimentary and volcanic facies recording the Neoarchaean continent breakup and decline of the positive δ13Ccarb excursion. Precambrian Res. https://doi.org/10.1016/j.precamres.2005.05.003

White, W.M., 2015. Radiogenic Isotope Geochemistry. Isotope geochemistry. John Wiley & Sons.

White, A.F., Brantley, S.L., 1995. Chemical Weathering Rates of Silicate Minerals: An Overview. Rev. Mineral. 31.

Wickman, F.E., 1948. Isotope Ratios: A Clue to the Age of Certain Marine Sediments. J. Geol. https://doi.org/10.1086/625478

Wierzbowski, H., Anczkiewicz, R., Bazarnik, J., Pawlak, J., 2012. Strontium isotope variations in Middle Jurassic (Late Bajocian-Callovian) seawater: Implications for Earth's tectonic activity and marine environments. Chem. Geol. https://doi.org/10.1016/j.chemgeo.2012.10.019

Workman, R.K., Hart, S.R., 2005. Major and trace element composition of the depleted MORB mantle (DMM). Earth Planet. Sci. Lett. 231, 53–72. https://doi.org/10.1016/ j.epsl.2004.12.005.

Windley, B.F., Kusky, T., Polat, A., 2021. Onset of plate tectonics by the Eoarchean. Precambrian Res. 352. https://doi.org/10.1016/j.precamres.2020.105980

Yoshioka, H., Asahara, Y., Tojo, B., Kawakami, S. ichi, 2003. Systematic variations in C, O, and Sr isotopes and elemental concentrations in neoproterozoic carbonates in Namibia: Implications for a glacial to interglacial transition. Precambrian Res. 124, 69–85. https://doi.org/10.1016/S0301-9268(03)00079-2

Young, G.M., 1991. The geological record of glaciation: relevance to the climatic history of Earth. Geosci. Canada.

Young, G.M., 2015. Environmental upheavals of the Ediacaran period and the Cambrian "explosion" of animal life. Geosci. Front. 6, 523–535. https://doi.org/10.1016/j. gsf.2014.09.001.

Young, G.M., 2019. Aspects of the Archean-Proterozoic transition: How the great Huronian Glacial Event was initiated by rift-related uplift and terminated at the riftdrift transition during break-up of Lauroscandia. Earth-Science Rev. 190, 171–189. https://doi.org/10.1016/j.earscirev.2018.12.013.

Young, S.A., Saltzman, M.R., Foland, K.A., Linder, J.S., Kump, L.R., 2009. A major drop in seawater 87Sr/86Sr during the Middle Ordovician (Darriwilian): Links to volcanism and climate? Geology 37. https://doi.org/10.1130/G30152A.1

Zhang, K., Zhu, X., Wood, R.A., Shi, Y., Gao, Z., Poulton, S.W., 2018. the evolution of complex eukaryotes. Nat. Geosci. 11. https://doi.org/10.1038/s41561-018-0111-y

Zhang, S., Wang, X., Wang, H., Bjerrum, C.J., Hammarlund, E.U., Costa, M.M., Connelly, J.N., Zhang, B., Su, J., Canfield, D.E., 2016. Sufficient oxygen for animal respiration 1,400 million years ago. Proc. Natl. Acad. Sci. U. S. A. 113, 1731–1736. https://doi.org/10.1073/pnas.1523449113

Zhang, Y., Yang, T., Hohl, S. V., Zhu, B., He, T., Pan, W., Chen, Y., Yao, X., Jiang, S., 2020. Seawater carbon and strontium isotope variations through the late Ediacaran to late Cambrian in the Tarim Basin. Precambrian Res. 345, 105769. https://doi.org/10.1016/j.precamres.2020.105769

Zhao, G., Cawood, P.A., Wilde, S.A., Sun, M., 2002. Review of global 2.1-1.8 Ga orogens: Implications for a pre-Rodinia supercontinent. Earth-Science Rev. https://doi.org/10.1016/S0012-8252(02)00073-9

Zhao, G., Sun, M., Wilde, S.A., Li, S., 2004. A Paleo-Mesoproterozoic supercontinent: Assembly, growth and breakup. Earth-Science Rev. 67, 91–123. https://doi.org/10.1016/j.earscirev.2004.02.003

Zhao, M.Y., Zheng, Y.F., Zhao, Y.Y., 2016. Seeking a geochemical identifier for authigenic carbonate. Nat. Commun. https://doi.org/10.1038/ncomms10885

Zhou, Y., von Strandmann, P.A.E.P., Zhu, M., Ling, H., Manning, C., Li, D., He, T., Shields, G.A., 2020. Reconstructing tonian seawater 87Sr/86Sr using calcite microspar. Geology 48, 462–467. https://doi.org/10.1130/G46756.1

Zhu, S., Zhu, M., Knoll, A.H., Yin, Z., Zhao, F., Sun, S., Qu, Y., Shi, M., Liu, H., 2016. Decimetre-scale multicellular eukaryotes from the 1.56-billion-year-old Gaoyuzhuang Formation in North China. Nat. Commun. 7. https://doi.org/10.1038/ncomms11500

Zhu, Z., Campbell, I.H., Allen, C.M., Burnham, A.D., 2020. S-type granites: Their origin and distribution through time as determined from detrital zircons. Earth Planet. Sci. Lett. 536. https://doi.org/10.1016/j.epsl.2020.116140

Figures

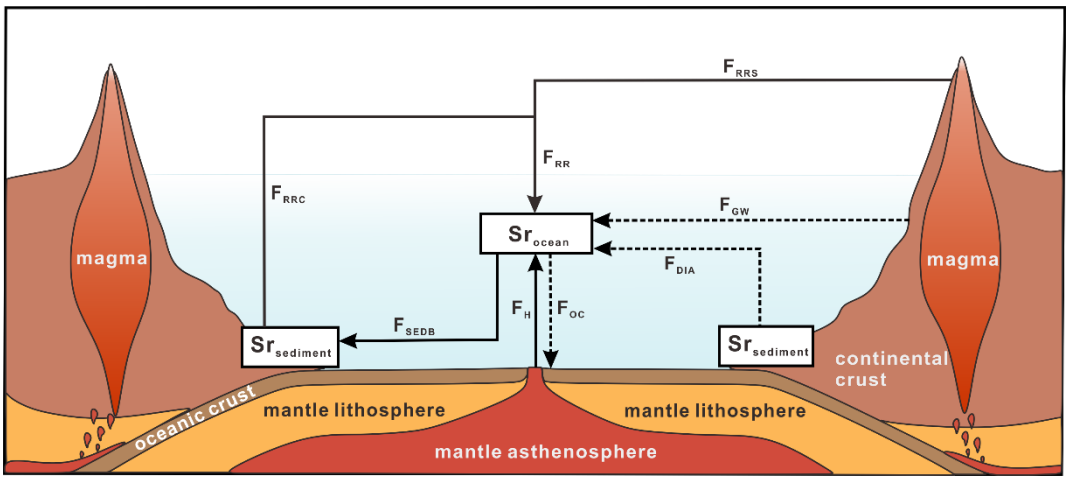

Fig. 1. Conceptual model of the seawater Sr fluxes cycle. Major sources of seawater Sr budget include radiogenic river runoff (F_{RR}) and unradiogenic hydrothermal input (F_H). River runoff (F_{RR}) can be divided into chemical weathering of silicate minerals (F_{RRS}) and dissolution of marine sediments (F_{RRC}). Other (minor) Sr seawater sources include ground water runout (F_{GW}), diagenetic reflux of Sr from recrystallization of sediments and buried pore water (F_{DIA}). At steady state, sources of seawater Sr are counteracted by removal of Sr via marine sediment burial (F_{SEDB}) and oceanic crust -seawater interaction (F_{OC}). Solid lines represent major Sr fluxes, and dash lines represent minor Sr fluxes. Boxes show reservoirs and arrows show fluxes.

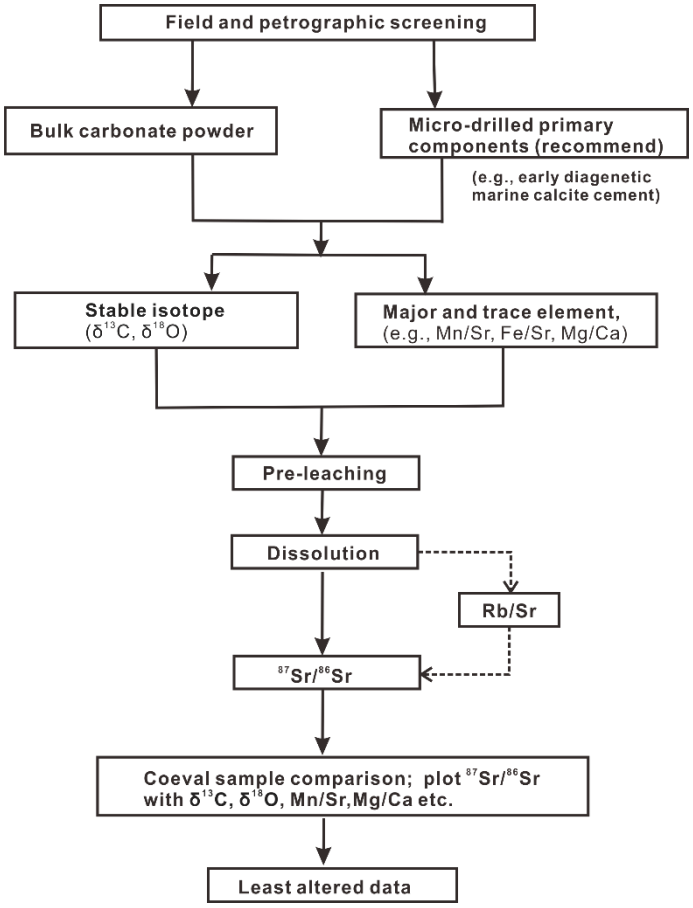

Fig.2. A recommended procedure for selecting the least altered $^{87}Sr/^{86}Sr$ data for SIS (Strontium isotope stratigraphy).

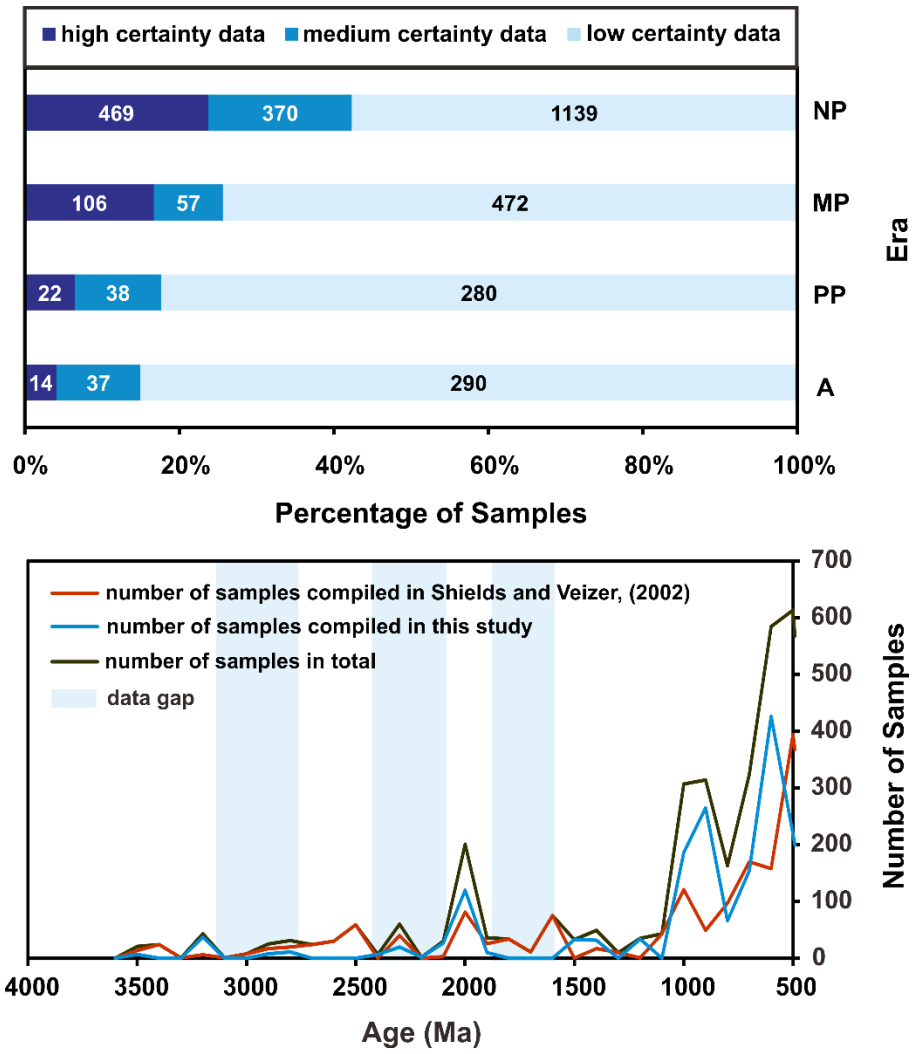

Fig. 3. Certainty and quantity distribution of samples from the Neoproterozoic to Archean. A) Data certainty versus eras. NP: Neoproterozoic, MP: Mesoproterozoic, PP: Paleoproterozoic, A: Archean. The Neoproterozoic has the most abundant high-certainty data. Low-certainty data occupy the largest proportions for all four periods. B) Quantity distribution of data from 500 Ma to 4000 Ma. Neoproterozoic era has relatively abundant datasets, but the Neoarchean, late Paleoproterozoic and Mesoproterozoic have relatively sparse datasets.

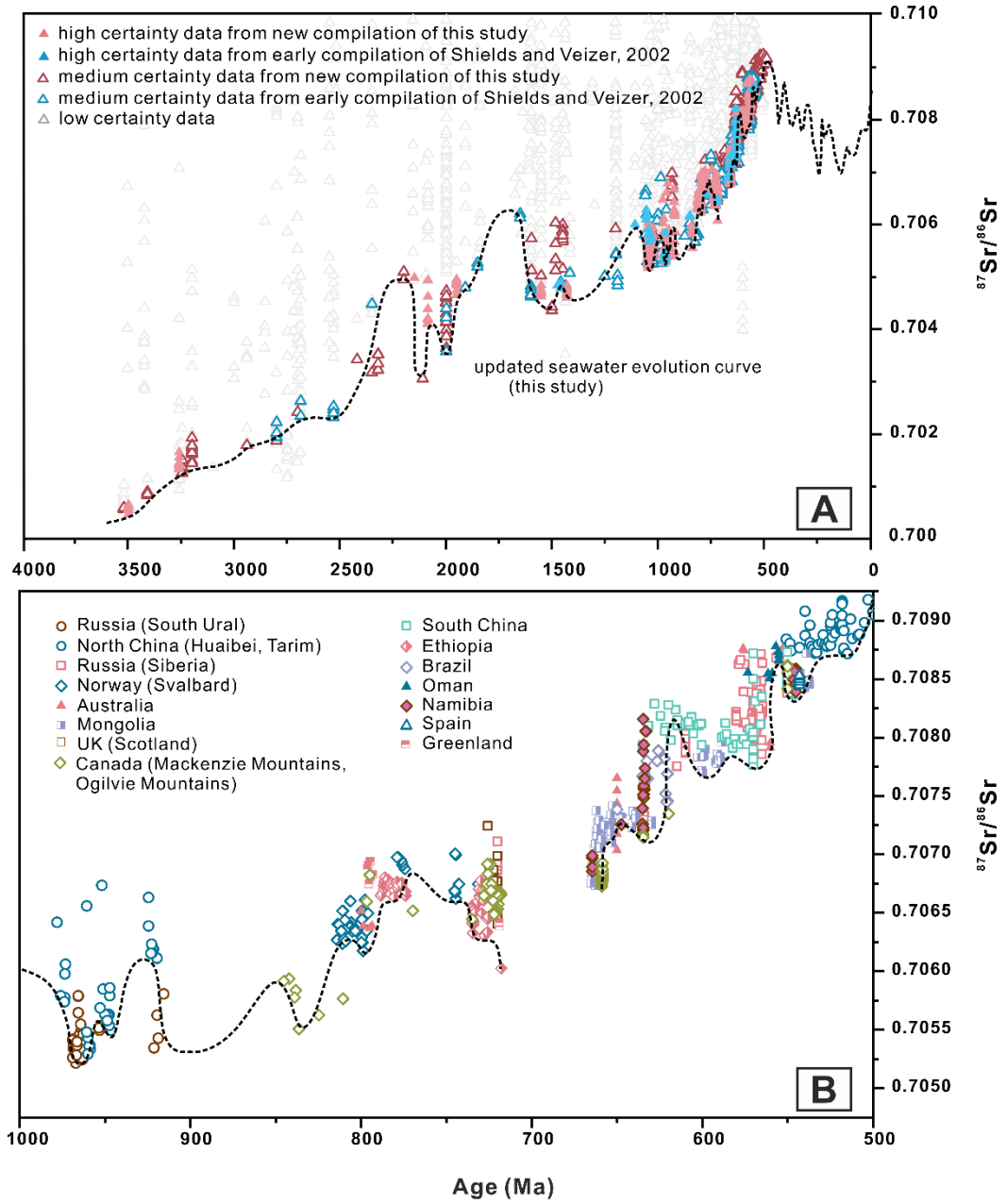

Fig. 4. The updated seawater $^{87}Sr/^{86}Sr$ curve with zoom-in image of the Neoproterozoic era. A) An updated strontium isotope curve of seawater. The Precambrian part is updated from this study, and the Phanerozoic part is from McArthur et al., (2020). B) A zoom-in image of Neoproterozoic strontium isotope curve from Fig.4A. The Neoproterozoic part is composed of well age constrained data in the high and medium certainty groups. The curve is updated from Zhou et al., (2020).

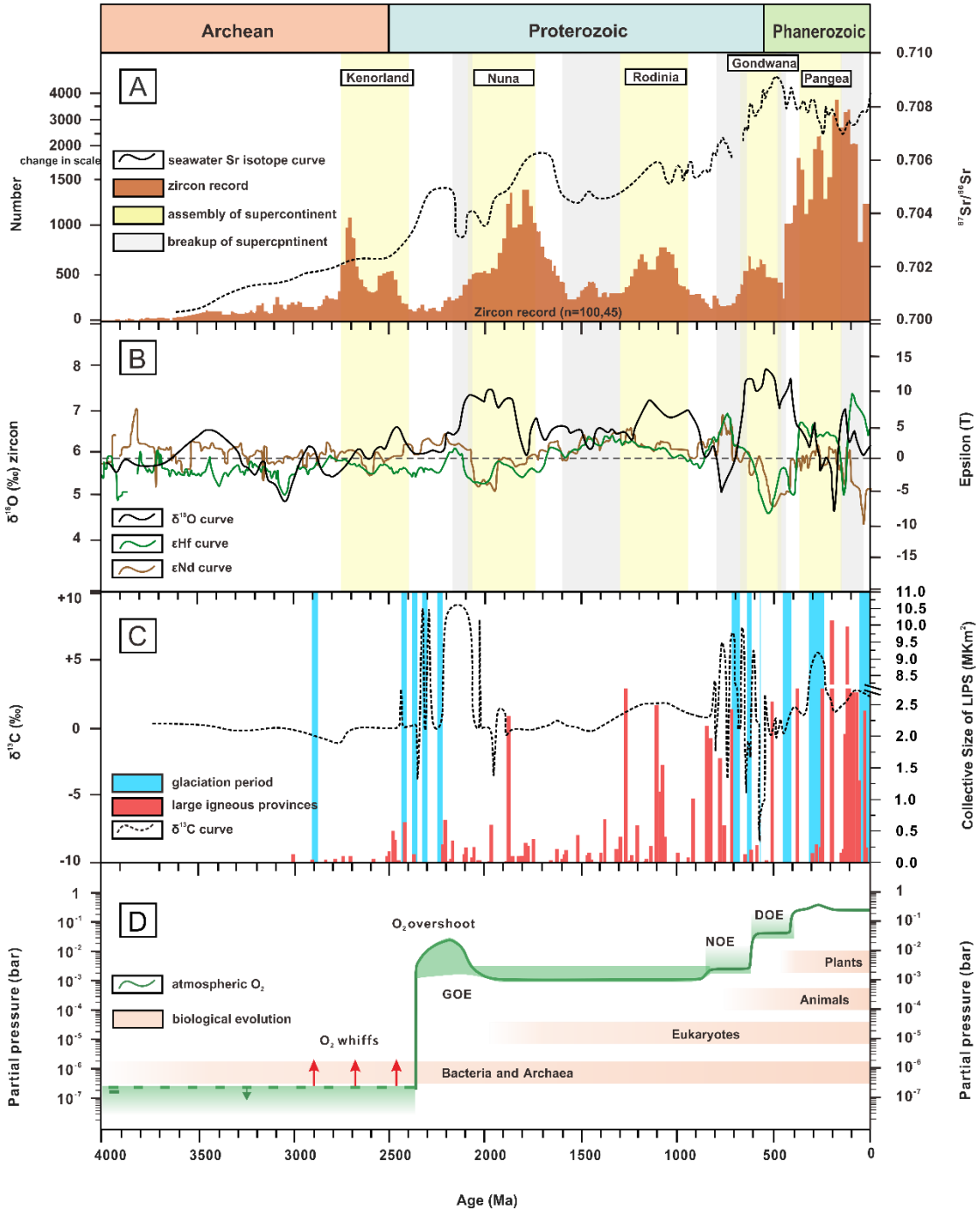

Fig. 5. An overview of the updated strontium isotope curve in the context of Earth systems evolution. A) The updated strontium isotope curve from this study couples zircon records from Voice et al., (2011) and supercontinental cycles. Periods of the supercontinent assembly are from Hawkesworth et al., (2016) and supercontinent breakups from Bradley, (2011); Condie, (2014); Condie and Puetz, (2019); Zhao et al., (2004). B) The black curve shows compilation of ~3300 $\delta^{18}O$ analyses of zircon

versus U-Pb age from recent sediments (Spencer et al., 2014). Green and brown lines represent median value of εHf for detrital zircons, εNd for whole-rock sediments and granitoids respectively (Condie et al., 2013). C) Vertical blue bars denote major glaciations during Earth's history (Young et al., 2019). Red bars show updated compilation of collective size of Large Igneous Provinces (LIPs) based on Ernst (2014), Ernst and Youbi (2017), and an updated compilation at http://www.largeigneousprovinces.org/. The $\delta^{13}C$ record throughout Earth history is compiled from Bekker et al., (2016), Hoffman and Lamothe, (2019) and Och and Shields-Zhou (2012). D) Schematic histories of atmospheric O_2 is from Catling and Zahnle (2020), which marks three major oxygenation events: GOE (Great Oxygenation Event), NOE (Neoproterozoic Oxygenation Event), and DOE (Devonian Oxygenation Event). Horizontal red bars shows evolution of life within the biosphere (Knoll and Nowak, 2017; Lenton et al., 2012).

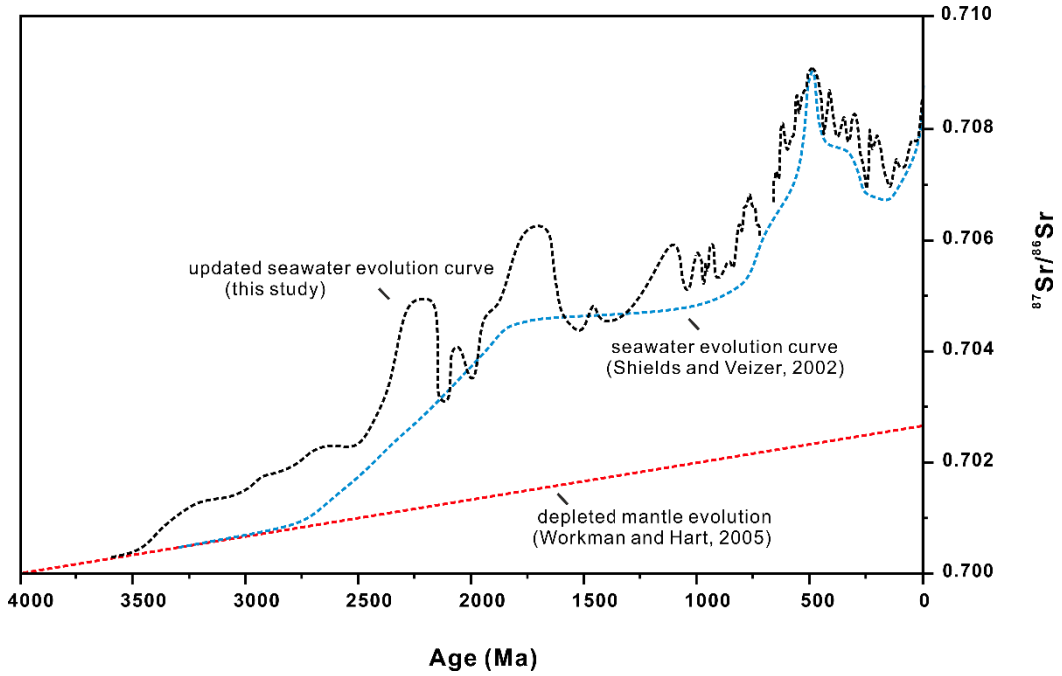

Fig.6. A comparison of updated Precambrian seawater $^{87}Sr/^{86}Sr$ curve from this study with that from Shields and Veizer (2002). The updated curve shows an earlier deviation from contemporaneous mantle and a stronger fluctuation than the curve from Shields and Veizer (2002). The depleted mantle evolution curve is from Workman and Hart (2005).